

# LOCAL MECHANISMS OF COMPOSITIONAL GENERALIZATION IN CONDITIONAL DIFFUSION

Arwen Bradley  
Apple  
Cupertino, CA

## ABSTRACT

Conditional diffusion models appear capable of compositional generalization, i.e., generating convincing samples for out-of-distribution combinations of conditioners, but the mechanisms underlying this ability remain unclear. To make this concrete, we study length generalization, the ability to generate images with more objects than seen during training. In a controlled CLEVR setting (Johnson et al., 2017), we find that length generalization is achievable in some cases but not others, suggesting that models only sometimes learn the underlying compositional structure. We then investigate locality as a structural mechanism for compositional generalization. Prior works proposed score locality as a mechanism for creativity in unconditional diffusion models (Kamb & Ganguli, 2024; Niedoba et al., 2024), but did not address flexible conditioning or compositional generalization. In this paper, we prove an exact equivalence between a specific compositional structure (*conditional projective composition*) (Bradley et al., 2025) and scores with sparse dependencies on both pixels and conditioners (*local conditional scores*). This theory also extends to feature-space compositionality. We validate our theory empirically: CLEVR models that succeed at length generalization exhibit local conditional scores, while those that fail do not. Furthermore, we show that a causal intervention explicitly enforcing local conditional scores restores length generalization in a previously failing model. Finally, we investigate feature-space compositionality in color-conditioned CLEVR, and find preliminary evidence of compositional structure in SDXL.

## 1 INTRODUCTION

Conditional diffusion models (Sohl-Dickstein et al., 2015; Ho et al., 2020; Song & Ermon, 2019; Song et al., 2020) appear to possess remarkable compositional generalization capabilities. For example, text-to-image models (Dhariwal & Nichol, 2021; Rombach et al., 2022; Ramesh et al., 2022) generate convincing images for prompts like “a photograph of a cat eating sushi with chopsticks” that were (probably) not seen during training. These models may generalize by composing known concepts (e.g. cat+sushi) in novel ways. However, the extent of generalization in large-scale models is unclear as their train sets are not publicly known (perhaps they *have* seen cats eating sushi). Further, despite recent progress (Okawa et al., 2024; Park et al., 2024; Sclocchi et al., 2025; Kadkhodaie et al., 2023; Favero et al., 2025; Chen et al., 2024; Wang et al., 2024; Lukoianov et al., 2025), the mechanisms underlying compositional generalization remain unclear.

We first propose a concrete and controlled setting in which to study compositional generalization: length generalization in location-conditioned models trained on CLEVR Johnson et al. (2017), a synthetic dataset of objects with various locations, shapes, and colors. Length generalization refers to the ability to generate more objects than seen in training – e.g., can a location-conditioned model trained on 1-3 objects and tested on  $K > 3$  locations actually generate images with  $K$  objects at the correct locations? Prior work demonstrated length generalization of *explicit* composition of multiple diffusion models via linear score combination Du et al. (2023); Liu et al. (2022); Bradley et al. (2025). In contrast, we study length generalization of a *single* conditional model. By training on multi-object samples, we hope that this model can learn the underlying compositional structure of the data, hence length-generalize. We find empirically that, depending on the conditioning specifics, these models sometimes length-generalize and sometimes do not.

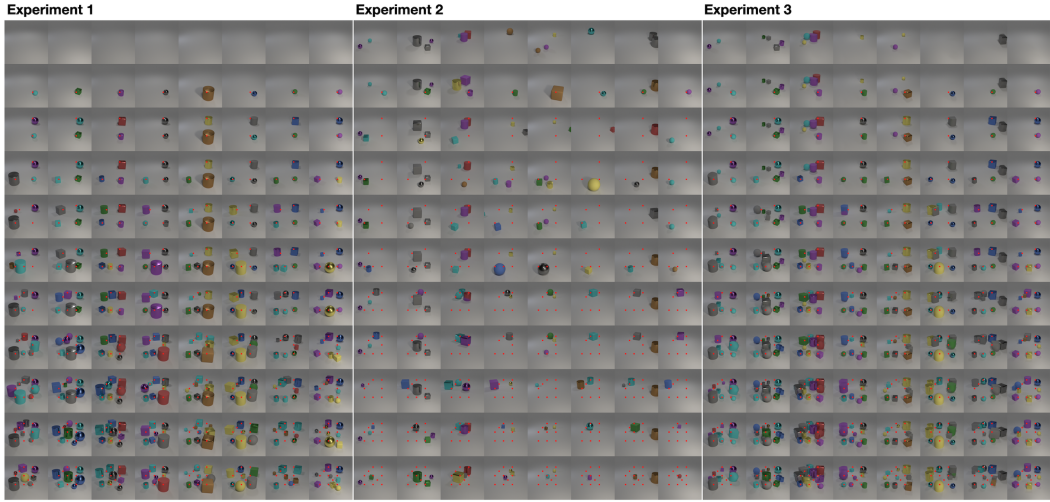


Figure 1: **Length generalization in location-conditioned CLEVR models.** We study length generalization in location-conditioned models trained on images with 1-3 objects, and tested on 0-10 locations (0 and  $\geq 4$  locations are out-of-distribution), with red dots indicating the conditioned locations at test-time. Experiments 1 and 2 have identical architectures and training data and differ only in the design of their conditioners. In **Experiment 1**, the conditioner labels the locations of all objects in the scene; the model successfully length-generalizes up to 9 locations (including 0). In **Experiment 2**, the conditioner labels the location of only a single object (randomly selected); the model largely fails to length-generalize. **Experiment 3** attempts to “fix” Exp. 2 with a causal intervention: we modify the model architecture to explicitly enforce local conditional scores, use the same training data and conditioning as Exp. 2, and find that length generalization is restored.

Next, we study local mechanisms for compositional generalization. We build primarily on two lines of prior work: one on local mechanisms for creativity, and another on compositionality in diffusion. First, Kamb & Ganguli (2024); Niedoba et al. (2024) recently proposed that models learn *local score functions*, enabling creativity via mosaicing of local patches from different images. These works only study unconditional and class-conditional diffusion, however, and do not consider flexible conditioners such as those used in text-to-image diffusion, which are central to questions of compositional generalization. Also, they empirically observe delocalization in trained score networks at high noise, when global scene structure is often resolved (Wang & Vastola, 2023). It therefore remains unclear whether local mechanisms are relevant to compositional generalization in conditional diffusion models. Second, Bradley et al. (2025) propose a formal definition, called *projective composition*, of “correct” composition of multiple distributions Du et al. (2023); Liu et al. (2022). In this paper, we specialize projective composition to a single conditional distribution to provide a precise definition of composition structure.

We develop a theoretical framework connecting compositional generalization with local mechanisms. Specifically, we generalize the concept of local scores to define *local conditional scores*: scores with *sparse dependencies* on both pixels and conditioners. That is, the score at a given pixel depends only on a subset of other pixels (such as a local neighborhood) and on only one or a few relevant conditioners (e.g. in the case of location-conditioning, only conditioners near the current pixel). We specialize projective composition (Bradley et al., 2025) to define a *conditional projective composition* – a conditional distribution that is a projective composition of its own individual conditionals. We then prove an equivalence between conditional projective composition and local conditional scores at all noise levels. We extend this theoretical framework to relate compositional structure and sparse score dependencies in feature-space (intuitively, if concepts like style+content compose in an appropriate disentangled feature space, then the score of each ‘style feature’ depends only on a sparse set of conditioners and other features related to style).

We validate this theory through experiments. Returning to our location-conditioned CLEVR setting and comparing a model that we found to length-generalize with one that did not, we find that both models maintain pixel-locality (even at high noise levels, in contrast to CIFAR-10 and other models

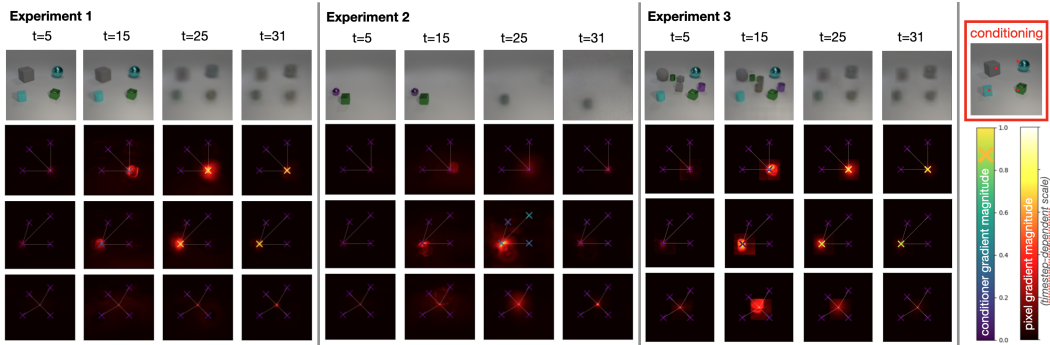


Figure 2: **Locality structures in location-conditioned CLEVR models** (Experiments 1, 2, 3 of Figure 1). All models are conditioned on 4 locations (OOD). Each column represents a timestep  $t$ . Top row shows the predicted denoised images via learned scores. Lower rows (evaluated at two conditioned and one unconditioned location) show heatmaps of the pixel gradient magnitude (average absolute of Jacobian from one pixel to all other pixels), and the conditional gradient magnitude marked with  $\times$  (with the “gradient” estimated via a finite difference of the score computed with and without each conditioner). Locality metrics are shown in Figure 10. All models show pixel-locality at low and high noise. The length-generalizing Experiment 1 model exhibits strong conditional-locality at high noise, while the non-length-generalizing Experiment 2 model critically lacks conditional-locality: the scores at conditioned locations either ignore all conditioners or depend on non-local conditioners. Experiment 3 model has architecturally-enforced local conditional scores, which restore length generalization. These experiments support the theoretical equivalence between CPC and LCS, and highlight the importance of conditional-locality at high noise.

studied by Kamb & Ganguli (2024); Niedoba et al. (2024)). However, the length-generalizing model has sparse dependencies on its location-conditioners while the non-length-generalizing model does not. Further, we perform a direct causal intervention to test local conditional scores as a possible mechanism for composition generalization: we show that explicitly enforcing a local architecture restores length generalization in the model that previously failed. Finally, we investigate feature-space compositionality in color-conditioned CLEVR, and show preliminary SDXL experiments to explore compositional structure in real-world text-to-image models.

## 2 LENGTH GENERALIZATION IN CLEVR

In this section we study length generalization in conditional diffusion models trained on CLEVR datasets Johnson et al. (2017), using a standard EDM2 U-net architecture Karras et al. (2022) (details in Section E.1). Figure 1 shows length generalization or lack thereof in two location-conditioned models trained on CLEVR images with 1-3 objects. In **Experiment 1**, the location-conditioning labels *all* objects in the scene, using a 2d integer array representing a 2d grid over the image via the count of objects whose center falls within the grid cell (typically zero or one), as shown in Figure 9. We find that this model successfully length-generalizes up to 9 objects, indicating that it has learned the underlying compositional structure of the data. In **Experiment 2**, however, length generalization fails. The setup is identical to that of Experiment 1 except for one difference: the conditioning only labels the location of a *single* randomly-selected object. (By analogy to text-

Train data	Exp. 1	Exp. 2	Exp. 3	Color
1 object	1	1	6	1
1-2 objects	5	1+(0-1)		
1-3 objects	9	1+(0-2)	9+(0-2)	4
1-4 objects	10	1+(0-3)		
1-5 objects	10	1+(0-4)	10+(0-2)	7
1-6 objects	11	1+(0-5)		

Table 1: **Limits of length generalization** in location- and color-conditioned CLEVR. The table lists the maximum value,  $K_{\max}$ , such that the model “succeeds” for every  $1 \leq K \leq K_{\max}$  (Section E.2). Exp. 1,2,3 refer to the location-conditioning experiments in Figure 1, Color refers to color-conditioning as in Figure 5. Parentheses e.g. +(0-2) indicate extra objects; untested configurations are left blank.

to-image conditioning, this difference is like text describing everything in each image vs. describing a single object in each image.) Since Experiment 2 conditions on only one location during training, there are at least two strategies that could perfectly fit the training data: draw an object at *every* conditioned location (compositional), or draw an object at *any* conditioned location (non-compositional). However, these strategies are *not* equivalent at inference time, when we condition on more than one location. The model evidently chooses a non-compositional strategy that fits the training data but does not length-generalize. **Experiment 3** “fixes” Experiment 2 via a local causal intervention motivated by our theory, as we discuss in Section 4 (note that since this model was trained on 1-3 object with only one location labeled, the expected inference-time behavior is to draw an object at each conditioned location, plus 0-2 extra objects). We also explore color-conditioning in CLEVR in Figure 5, which we expect to have a compositional structure in an appropriate feature-space, discussed further in Section 4. Table 1 gives a quantitative analysis of the limits of length generalization of the various location- and color-conditioned models, trained on 1 to  $M$  objects for  $M = 1, \dots, 6$  (Exp. 1 samples in Figure 8). The table reports an approximate measure of the maximum number of objects to which each model can consistently length-generalize (details in Section E.2).

### 3 THEORY: COMPOSITIONALITY AND LOCALITY

In this section we present theory connecting compositional generalization to generalized local mechanisms. We first define *local conditional scores* (LCS), an extension of local scores Kamb & Ganguli (2024); Niedoba et al. (2024) to account for flexible conditioners. An LCS evaluated at a given pixel has sparse dependencies on other pixels (generalizing local neighborhoods) and sparse dependencies on conditioners. Next, we define *conditional projective composition* (CPC), a special case of *projective composition* (PC) proposed in Bradley et al. (2025) applied to a single conditional distribution. A conditional distribution that satisfies CPC factorizes into independent distributions over disjoint subsets of pixels that depend on a single conditioner. LCS and CPC are illustrated in Figure 3. We then prove that the score of a CPC is exactly an LCS: intuitively, *compositional distributions have local scores*. This result can be partially relaxed in an approximation that improves at higher noise, which could allow approximately-compositional structure to be resolved early in denoising. The theory can also be extended to *feature space*, to connect compositional structure (e.g. style+content) with sparse score dependencies (e.g. scores of ‘style features’ only depend on select conditioners and features relevant to style). The remainder of this section makes these claims precise.

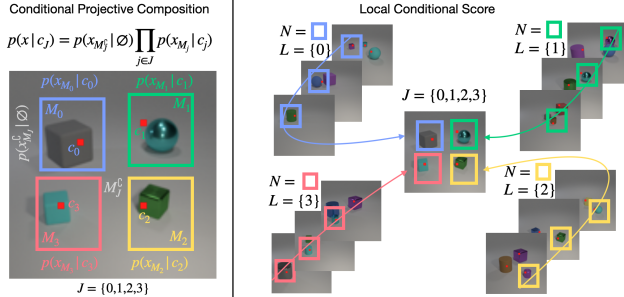


Figure 3: *Conditional projective composition* (CPC) and *local conditional scores* (LCS). A CPC is a conditional distribution over a set of conditions  $c_{\mathcal{J}}$  that factorizes independently into the marginals over  $x_{M_j}$  conditioned on  $c_j$ , where  $M_j$  are disjoint subsets. An LCS is a conditional score over a set of conditions  $c_{\mathcal{J}}$  such that the score at each pixel  $i$  depends only on a subset  $N_i$  of other pixels (often a local neighborhood) as well as a subset  $L_i \subset \mathcal{J}$  of conditions (for location-conditioning, often nearby conditioners). For certain choices of subsets, CPC and LCS are equivalent.

**Local Conditional Scores** We generalize the idea of local scores (Kamb & Ganguli, 2024; Niedoba et al., 2024) to account for flexible compositional conditioners,<sup>1</sup> which are central to compositional generalization. Let  $p(x|c)$  be the true distribution over data  $x \in \mathbb{R}^n$  conditioned on  $c$ . Let  $x_N$  denote the restriction of  $x$  to a subset of indices  $N \subseteq [n]$ , and  $p(x_N|c)$  denote the marginal distribution of  $p(\cdot|c)$  on  $x_N$ . Conditioners are represented as  $c_{\mathcal{J}} = \{c_j, j \in \mathcal{J}\}$ , where  $\mathcal{J} \subseteq \mathcal{J}_{\text{all}}$  is a subset of all possible conditioners. We assume that  $p$  is defined for any combination of conditioners,

<sup>1</sup>Our definition breaks slightly from the originals in defining local scores in terms of a distribution rather than a finite training set, and also omits equivariance, which is unnecessary for our theory.

even those not seen during training. A local conditional score at pixel  $i$ ,  $s^t[x|c_{\mathcal{J}}](i)$ , depends on two subsets (Figure 3):  $N_i$ , a subset of pixels relevant to pixel  $i$ , and  $L_i(\mathcal{J})$ , a subset of conditions in  $\mathcal{J}$  relevant to pixel  $i$ . In general, the subsets  $N_i$  and  $L_i$  need not be disjoint (although this will later be necessary to achieve CPC equivalence), and may contain multiple objects or conditioners.

**Definition 1** (Local Conditional Score (LCS)). *We say that  $s^t$  is a local conditional score at time  $t$  with pixel subsets  $N_i$  and conditional subsets  $L_i^t$  (which may both depend on the time  $t$ ), if*

$$s^t[x|c_{\mathcal{J}}](i) := \nabla \log p^t[x_{N_i^t}|c_{L_i^t(\mathcal{J})}](i). \quad (1)$$

Importantly, Definition 1 does not strictly require “locality” but rather captures a “sparse dependency structure” where the score at index  $i$  depends only on specific subsets  $N_i$  and  $L_i$ . While  $N_i$  is often a local neighborhood in image settings (and  $L_i$  can be local e.g. for location-conditioners), these subsets can be arbitrary in general. We use “local” as an intuitive term for these sparse dependencies.

**Conditional Projective Composition** To define a compositional structure for conditional distributions, we introduce conditional projective composition (CPC). We do not claim all distributions have this structure, but we will show that those that do also have a local score structure (LCS), suggesting a mechanism for compositional generalization. We specialize Bradley et al. (2025)’s pixel-space projective composition to the case where the concept distributions  $p_j$  represent the a *single* conditional distribution  $p(x|c_j)$  conditioned on different  $c_j$ , and the background distribution  $p_b(x)$  is  $p(x|\emptyset)$  (i.e., with no conditioners active).

**Definition 2** ((Pixel-space) Conditional Projective Composition (CPC)). *We say that  $p(x|c)$  is a conditional projective composition if there exist disjoint sets  $M_j$  for all conditions  $j \in \mathcal{J}_{all}$  such that, for any set of conditions  $\mathcal{J} \in \mathcal{J}_{all}$ ,  $p(x|c_{\mathcal{J}})$  decomposes as*

$$p(x|c_{\mathcal{J}}) := p(x_{M_{\mathcal{J}}^c}|\emptyset) \prod_{j \in \mathcal{J}} p(x_{M_j}|c_j), \quad (2)$$

where  $M_{\mathcal{J}}^c := \mathbb{R}^n \setminus \cup_{j \in \mathcal{J}} M_j$  denotes the set of pixels not controlled by any active condition.

This definition means that the conditional distribution  $p$  decomposes into independent marginal distributions  $p(x_{M_j}|c_j)$ , each depending only on subset  $M_j$  and condition  $c_j$ , as shown in Figure 3. That is,  $p$  modifies  $M_j$  according to  $c_j$  independently of other pixel sets and conditioners. This condition is quite strong, but we will partially relax it in our theory.

### 3.1 EQUIVALENCE BETWEEN COMPOSITIONAL STRUCTURE AND LOCAL SCORES

In this section we present theory showing that the score of an (approximately) conditional projective composition is (approximately) a particular local conditional score. We begin by showing that a specific local conditional score is *exact* for a conditional projective composition.

**Lemma 1** (Local conditional score is exact for conditional projective composition). *Let  $p$  be a pixel-space CPC (Definition 2) with disjoint sets  $\{M_j\}$ . Let  $s^t$  be an LCS (Definition 1) with subsets:*

$$L_i^t(\mathcal{J}) = \begin{cases} \{j\} \cap \mathcal{J}, & \text{if } i \in M_j \\ \emptyset, & \text{else,} \end{cases} \quad \text{and} \quad N_i^t = \begin{cases} M_j, & \text{if } i \in M_j \\ M_b, & \text{else,} \end{cases} \quad \text{where } M_b := M_{\mathcal{J}_{all}}^c.$$

*Then  $s^t$  is exactly the score of  $p^t$ :*

$$s^t(x|c_{\mathcal{J}}) = \nabla \log p^t(x|c_{\mathcal{J}}), \quad \forall \mathcal{J}.$$

The proof is in Section B. The lemma says that when the locality structure of  $s^t$  is precisely connected to the compositional structure of  $p^t$  – intuitively, when pixel  $i$  belongs to the subset  $M_j$  controlled by condition  $j$  in the CPC, then  $L_i = \{j\}$  (pixel  $i$  only depends on condition  $j$ ), and  $N_i = M_j$  (pixel  $i$  only depends on pixels in  $M_j$ ) – then  $s^t$  is exactly the score of  $p^t$ . Thus, there is an *equivalence* between CPCs and LCSs. This is illustrated in Figure 3.

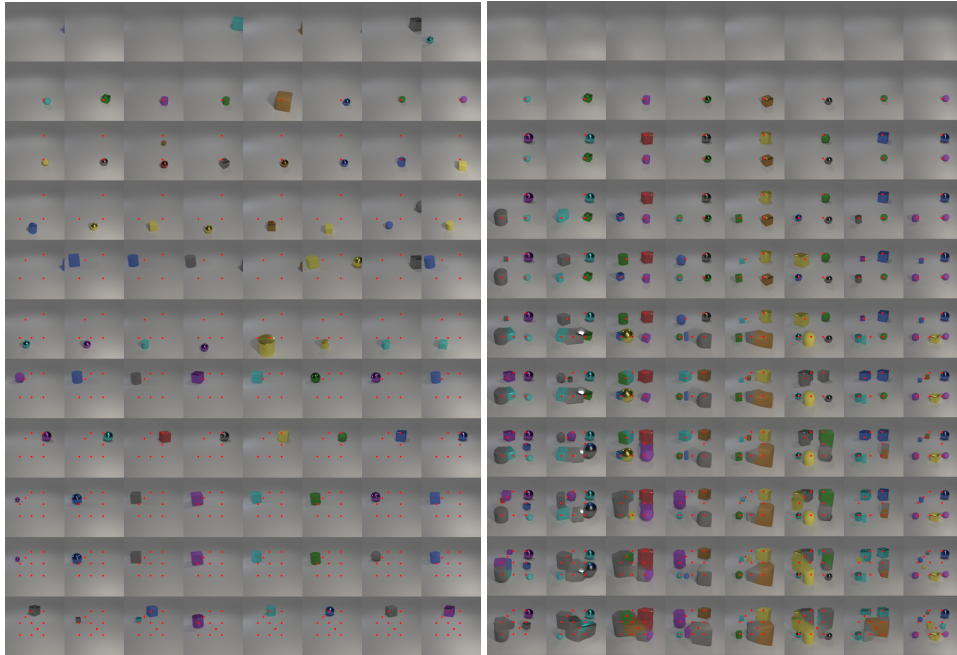


Figure 4: **Local causal intervention enables length generalization in location-conditioned model trained on a single object.** We test length generalization in two location-conditioned models trained on images with only a *single* object (and conditioned on its single location). Left: A model with the standard EDM2 architecture of Experiment 1 does not length-generalize: it always generates exactly one object (even when conditioned on zero locations). Right: A model with the explicitly-enforced local architecture of Experiment 3 (see Section E.3) length-generalizes up to 6 objects, albeit with some artifacts (objects “merging” into each other). Although it does not perform as well as the Exp. 3 local model trained on 1-3 objects (Figure 1), any length-generalization after training on only one object is remarkable. (In Section E.2, we hypothesize that training on more objects, e.g. 1-3, may improve length-generalization by allowing the model to learn *clusters* of objects).

**A relaxation** What about imperfect compositionality? We can relax Lemma 1 to show that the score of an *approximately* CPC distribution is *approximately* an LCS. Further, we show that the CPC approximation becomes more accurate – intuitively, distributions are “more compositional” – at higher noise. The precise statements and proofs are given in Section C. Why might this be helpful? If conditional dependencies are strongest at high noise and pixel dependencies take over at low noise (as we observe in Figure 2), then local conditional mechanisms might be able to establish large-scale compositional structure (like object count and location) early in denoising, leaving less-compositional details to be resolved at low noise via local unconditional denoising.

### 3.2 FEATURE-SPACE CONDITIONAL PROJECTIVE COMPOSITION

What if CPC does *not* hold in pixel-space – as is typically the case for non-location conditioners, like the color-conditioning of Figure 5, or text-to-image prompts such as “a watercolor of a cat eating sushi with chopsticks”? Pixel-space CPC is unlikely since each condition potentially affects many pixels (e.g., “watercolor” style would apply to all pixels). In these cases, we hypothesize that the local unconditional denoising mechanism still applies at low noise (Kamb & Ganguli, 2024; Niedoba et al., 2024). But is there any hope of compositional generalization at high noise?

It follows directly from Lemma 1 that if a distribution has a CPC structure *in feature-space* then its score is an LCS *in feature-space*:

**Corollary 1** (LCS is exact for CPC in feature-space). *Suppose that  $p(x|c)$  is a CPC in an appropriate feature-space: that is,  $\mathcal{A}\#p(z|c)$  is a CPC, where  $\mathcal{A}$  is an invertible feature-space transform, and  $z := \mathcal{A}(x)$  is the feature-space representation. Then the feature-space score  $\nabla_z \log(\mathcal{A}\#p)^t(z|c)$  is an LCS with neighborhoods  $N_i, L_i$  related to the CPC subsets  $\{M_j\}$  of  $\mathcal{A}\#p$  as in Lemma 1.*

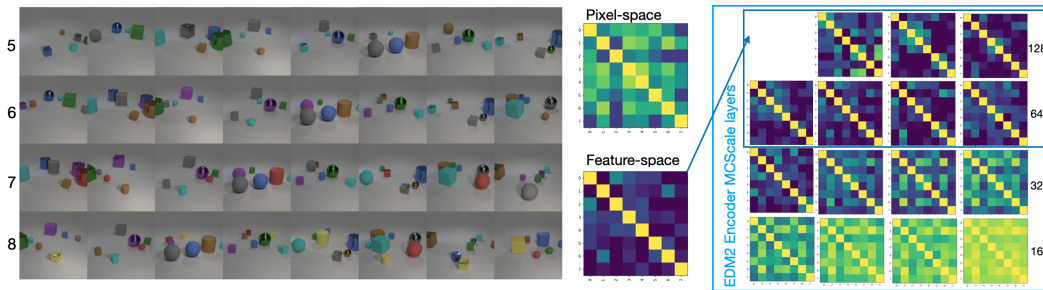


Figure 5: **Length generalization in color-conditioned CLEVR.** (Left) We test length generalization in a CLEVR model conditioned on *colors* (rather than locations), trained on 1-5 objects. We test up to 8 colors (blue, brown, cyan, gray, green, purple, red, yellow), and find generalization up to 7 colors, suggesting that compositional structure may exist in a learned feature-space. (Right) We visualize disentanglement between individual colors in the network’s internal representation via the cosine similarity heuristic 3 (low similarity off-diagonal indicates disentanglement). Colors seem to be significantly disentangled in early encoder layer activations – which may form a compositional “feature-space” potentially promoting generalization.

For example, an appropriate feature-space mapping might disentangle the concepts “watercolor”, “cat”, and “sushi” into the required CPC structure – even though these concepts interact in pixel space. (Note that defining LCS in terms of “sparse dependencies” rather than literal “locality” is essential in feature-space, where conditioners are not locations and interacting features need not be contiguous). However, challenges remain: if the scores are LCS in feature-space, in order to exploit the sparse structure, the model must *learn* the associated feature-space mapping and its inverse, in addition to the local subsets, making the learning process significantly more challenging.<sup>2</sup> This argument is made precisely in Section D.

Finally, as a practical heuristic for identifying CPC structure in feature-space, we adapt a lemma of Bradley et al. (2025). In this context, it states that a necessary, but not sufficient, condition for CPC in a feature-space given by  $\mathcal{A}$  is orthogonality of the mean difference vectors in feature-space, i.e.

$$(\mu_i - \mu_b)^T (\mu_j - \mu_b), \quad \forall i \neq j, \quad \text{where } \mu_i := \mathbb{E}_{(\mathcal{A}\#p)(z|c_i)}[z], \quad \mu_b := \mathbb{E}_{(\mathcal{A}\#p)(z|\emptyset)}[z]. \quad (3)$$

To evaluate heuristic 3, we can construct a cosine similarity matrix  $\{d_i d_j / \|d_i\| \|d_j\|\}_{i,j}$ , with  $d_i = \mu_i - \mu_b$ : low similarity off-diagonal is evidence of feature-space disentanglement.

## 4 ADDITIONAL EXPERIMENTS

Our theory shows an equivalence between LCS and CPC (which leads to length generalization). We test this directly in location-conditioned CLEVR models, where the compositional structure holds in pixel-space, and location-conditioners possess a direct notion of locality. Further, we test whether LCS could be a *causal* mechanism via a direct intervention: enforcing an explicitly LCS architecture to “fix” length generalization that previously failed. Turning to feature-space compositionality, we show partial length generalization in color-conditioned CLEVR and connect it with feature-space disentanglement. Finally, we make preliminary investigations of compositional structure in both pixel- and feature-space in SDXL.

**Pixel-space locality in location-conditioned CLEVR** Figure 2 shows pixel- and conditional-locality in Experiments 1 and 2 (we will discuss Experiment 3 in the next section). We first observe that both models maintain pixel-locality at both low and high noise levels, contrasting with prior empirical findings on datasets like CIFAR-10 (Kamb & Ganguli, 2024; Niedoba et al., 2024) – reproduced in Figure 12 – showing delocalization at high noise. The difference likely stems from CLEVR images containing multiple, nearly- independent objects; unlike the datasets with a single centered

<sup>2</sup>In fact, even learning the feature-space transform and its inverse for the noiseless distribution is not enough – the model technically needs to learn a feature-map for every noise level. In practice it may be approximately sufficient to learn a single mapping and its inverse, though this is not entirely clear.

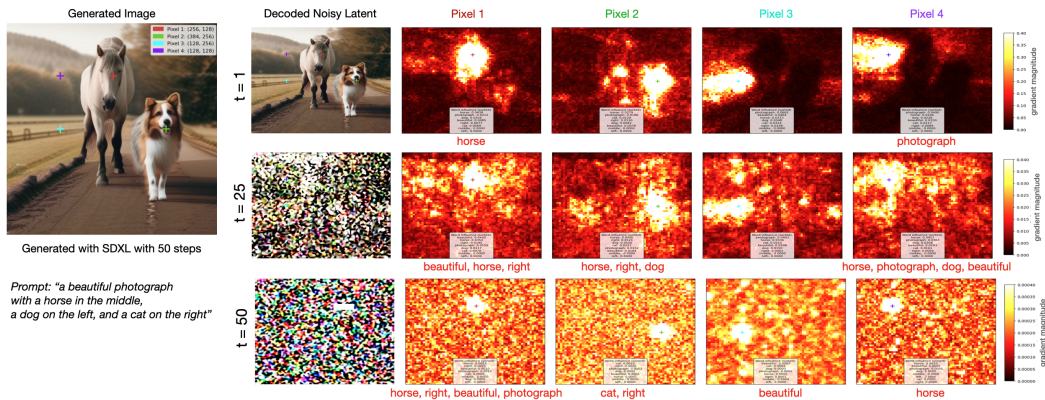


Figure 6: **Preliminary SDXL pixel-space locality study.** An SDXL generated image with the prompt “a beautiful photograph with a horse in the middle, a dog on the left, and a cat on the right.” Heatmaps show pixel gradient magnitude at locations marked with +. The conditional gradient magnitude w.r.t. individual words is also evaluated at the indicated pixel, with dominant words (if any) shown in red. SDXL shows *some degree* of pixel-locality (particularly at low noise) and *some degree* of conditional-locality (more so at higher noise); consistent with apparently only *some degree* of compositional generalization (note the failure to draw a cat).

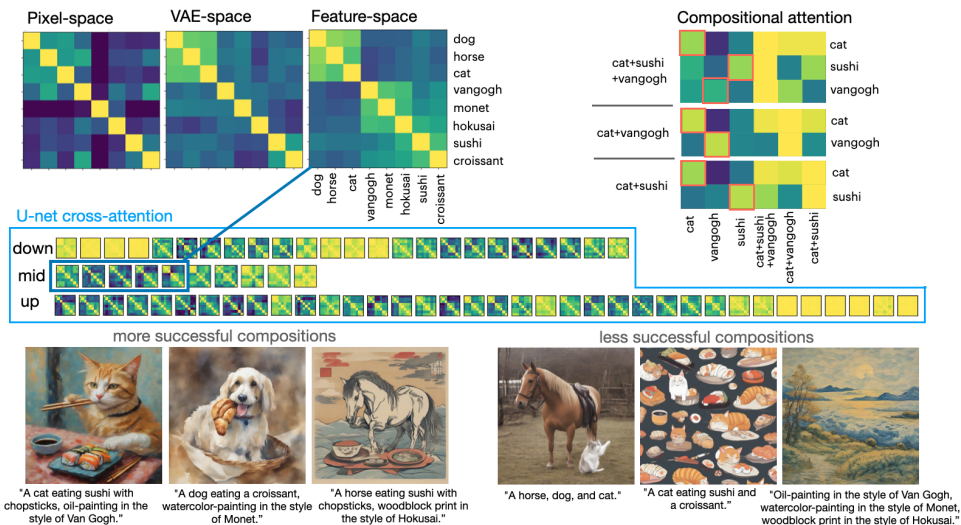


Figure 7: **Preliminary evidence for feature-space compositionality in SDXL** via cosine similarity heuristic 3. (Top): Disentanglement between concepts (“dog”, “horse”, “cat”, “van Gogh”, “Monet”, “Hokusai”, “sushi”, “croissant”). Pixel-space lacks meaningful structure, VAE-space exhibits some structure, and a clearer structure emerges within a proposed compositional Feature-space comprised of U-net mid block activations – showing high intra-group similarity (e.g. dog, horse, cat) and lower inter-group similarity (e.g. cat, van Gogh). Compositional attention maps show that within multi-concept prompts (e.g. cat+sushi+van Gogh), individual token (e.g. cat) activations have high similarity with corresponding single-concept (cat) activations, consistent with compositional structure. (Middle): Cosine similarities across all U-net cross-attention blocks (larger version in Figure 13). (Bottom): SDXL example generations. Disentangled concepts in the proposed feature-space (e.g. cat+sushi+van Gogh) compose more successfully than highly-entangled concepts (e.g. horse+dog+cat).

subject studied in prior work. Second, we note significant differences in conditional-locality between Experiments 1 and 2. The length-generalizing Exp. 1 model exhibits strong conditional-locality at high noise, while the non-length-generalizing Exp. 2 model lacks conditional-locality at high noise

---

(scores near conditioned locations either fail to respond to any conditions or depend on several non-local conditions). At low noise, both models transition to pixel-local *unconditional* denoising, as in Kamb & Ganguli (2024); Niedoba et al. (2024). These experiments support our prediction that length generalization depends on pixel- and conditional-locality, and suggest that conditional-locality at high noise plays a particularly important role. Details in Section F.

**A Causal Intervention in location-conditioned CLEVR** Experiment 3 (Figure 1) tests our theory via a direct causal intervention, wherein we design a local model architecture that explicitly enforces local conditional scores (as confirmed in Figure 2). We train the local model using the same conditioning as the failing Experiment 2 (labeling only a single object location), and find that the local architectural intervention restores length generalization (Table 1), “fixing” the failure. In fact, the local model trained on *only one object* can length-generalize up to 6 locations, unlike even the Exp. 1 model (Figure 4, Table 1). This supports the hypothesis that local conditional scores could be a *causal* mechanism for compositional generalization. Additional details in Section E.3.

**Length generalization in color-conditioned CLEVR** To better understand feature-space compositionality, we explore length generalization in color-conditioned CLEVR in Figure 5 and Table 1. For color-conditioning, we would expect compositional structure to exist in an appropriate feature space that disentangles the different colors. We observe that length generalization is possible to some extent – e.g. a model trained on 1-5 objects can generalize to 7 colors. Next, we investigate whether the model actually learns a feature space with CPC structure (Figure 5 right) by analyzing layer activations using the cosine similarity heuristic 3, and find evidence that colors are in fact significantly disentangled within several layers. Details in Section E.4.

**A preliminary SDXL investigation** Can local mechanisms help to explain compositional generalization in real-world diffusion text-to-image models? We begin to explore this question by studying compositional structure in both pixel- and feature-space in a pretrained (‘out-of-the-box’) SDXL model (Podell et al., 2023) model. In Figure 6, we investigate pixel-space locality, by choosing a prompt that contains implicit location information (“middle”, “right”, “left”). We find some degree of locality even at high noise, and somewhat sparse dependencies on the text conditioner (measured by splitting the prompt into individual words and computing the score delta as we ablate each word). For example, the region where the horse ends up being drawn has the strongest dependency on the word “horse” at most noise levels, similar to observations in Chefer et al. (2023); Hertz et al. (2022). The local structure is far from perfect, but notably so is the compositionality – it entirely fails to draw a cat as requested in the prompt. Details in Section G and F.

Next, we move beyond pixel-space to investigate whether SDXL may learn a compositional feature-space in its internal representation. Certain concepts, such as animals vs. art styles, are almost certainly entangled in pixel-space but might be disentangled within the network’s internal feature-space, enabling composition. We analyze U-net cross-attention layer activations using the cosine similarity heuristic 3, and find evidence of compositional structure within several layers of the mid-block: related concepts like dog, cat, and horse have high similarity, while concepts like cat and van-Gogh have much lower similarity. We also show examples connecting this feature-space structure with successful and unsuccessful compositions. Details in Section G.

## 5 DISCUSSION AND FUTURE WORK

Whether local mechanisms can explain compositional generalization in real-world diffusion models remains an open question. The preliminary SDXL experiments in Section 4 are meant only to be suggestive, and much more work is needed to fully understand compositional generalization in modern text-to-image models. This setting presents several challenges. First, since we often don’t know what was in the training set, it is unclear which prompts are actually OOD. Second, some kinds of compositional structure, such as style+content, exist only in feature-space, requiring more complex studies of the model’s learned representation as in Figures 5 and 7, potentially relying on heuristics such as 3. Despite significant evidence for feature disentanglement in diffusion representations (see Section A), this is still not fully understood. Future work could also exploit our finding of local conditional scores as a mechanism to improve compositional generalization. Our causal intervention in Experiment 3 shows that in a simple setting, enforcing an explicitly local architecture can im-

---

prove generalization, suggesting that similar architectural, training, or inference-based interventions might be able to improve real-world models. Several existing methods can be viewed as implicit “local interventions”: for instance, layout-to-image methods that use explicit local constraints or biases (see Section A), or more generally, sparse attention architectures Child et al. (2019); Sun et al. (2022). Our theory helps to explain why these approaches are beneficial, and suggests more precise ways to target compositional generalization by specifically enforcing local conditional scores. When compositional structure exists only in feature-space, such interventions become more complex. The challenge becomes two-fold: we must first identify – or attempt to induce – feature-space transformations that reveal the compositional structure, and then apply local interventions within the learned feature space. Larger-scale studies on complex, real-world datasets are essential to clarify the challenges and explore opportunities to improve compositional generalization via local interventions.

## 6 CONCLUSION

We proposed local conditional scores as a possible mechanism for compositional generalization. Theoretically, we proved an equivalence between conditional projective composition (a specific compositional structure) and local conditional scores (which capture both pixel- and conditional-locality); this theory extends to feature-space compositionality. Empirically, we verified that length generalization in location-conditioned CLEVR models corresponds with local conditional dependencies at high noise combined with pixel-locality at low noise. Then, we demonstrated through a causal intervention that enforcing a local architecture restores length generalization in a model that previously failed. We also offered evidence for feature-space compositionality in color-conditioned CLEVR, and preliminary evidence of compositional structure in both pixel- and feature-space in SDXL. Our results support local conditional scores as a potential mechanism of compositional generalization in conditional diffusion models, offering a lens to understand when and how generalization is achieved, and potential avenues to improve it.

### ACKNOWLEDGMENTS

We gratefully acknowledge Preetum Nakkiran, Miguel Angel Bautista, and Josh Susskind for helpful discussions and feedback throughout this project, and David Berthelot and James Thornton for developing code infrastructure supporting the CLEVR experiments.

### REFERENCES

- Quentin Bertrand, Anne Gagneux, Mathurin Massias, and Rémi Emonet. On the closed-form of flow matching: Generalization does not arise from target stochasticity. *arXiv preprint arXiv:2506.03719*, 2025.
- Arwen Bradley, Preetum Nakkiran, David Berthelot, James Thornton, and Joshua M Susskind. Mechanisms of projective composition of diffusion models. *arXiv preprint arXiv:2502.04549*, 2025.
- Hila Chefer, Yuval Alaluf, Yael Vinker, Lior Wolf, and Daniel Cohen-Or. Attend-and-excite: Attention-based semantic guidance for text-to-image diffusion models. *ACM transactions on Graphics (TOG)*, 42(4):1–10, 2023.
- Ricky TQ Chen, Xuechen Li, Roger B Grosse, and David K Duvenaud. Isolating sources of disentanglement in variational autoencoders. *Advances in neural information processing systems*, 31, 2018.
- Siyi Chen, Huijie Zhang, Minzhe Guo, Yifu Lu, Peng Wang, and Qing Qu. Exploring low-dimensional subspace in diffusion models for controllable image editing. *Advances in neural information processing systems*, 37:27340–27371, 2024.
- Jiaxin Cheng, Xiao Liang, Xingjian Shi, Tong He, Tianjun Xiao, and Mu Li. Layoutdiffuse: Adapting foundational diffusion models for layout-to-image generation. *arXiv preprint arXiv:2302.08908*, 2023.

- 
- Jiaxin Cheng, Zixu Zhao, Tong He, Tianjun Xiao, Zheng Zhang, and Yicong Zhou. Rethinking the training and evaluation of rich-context layout-to-image generation. *Advances in Neural Information Processing Systems*, 37:62083–62107, 2024.
- Rewon Child, Scott Gray, Alec Radford, and Ilya Sutskever. Generating long sequences with sparse transformers. *arXiv preprint arXiv:1904.10509*, 2019.
- Omer Dahary, Or Patashnik, Kfir Aberman, and Daniel Cohen-Or. Be yourself: Bounded attention for multi-subject text-to-image generation. In *European Conference on Computer Vision*, pp. 432–448. Springer, 2024.
- Prafulla Dhariwal and Alexander Nichol. Diffusion models beat gans on image synthesis. *Advances in neural information processing systems*, 34:8780–8794, 2021.
- Yilun Du and Leslie Pack Kaelbling. Position: Compositional generative modeling: A single model is not all you need. In *Forty-first International Conference on Machine Learning*, 2024.
- Yilun Du, Conor Durkan, Robin Strudel, Joshua B Tenenbaum, Sander Dieleman, Rob Fergus, Jascha Sohl-Dickstein, Arnaud Doucet, and Will Sussman Grathwohl. Reduce, reuse, recycle: Compositional generation with energy-based diffusion models and mcmc. In *International conference on machine learning*, pp. 8489–8510. PMLR, 2023.
- Alessandro Favero, Antonio Sclocchi, Francesco Cagnetta, Pascal Frossard, and Matthieu Wyart. How compositional generalization and creativity improve as diffusion models are trained. *arXiv preprint arXiv:2502.12089*, 2025.
- Leon A Gatys, Alexander S Ecker, and Matthias Bethge. Image style transfer using convolutional neural networks. In *Proceedings of the IEEE conference on computer vision and pattern recognition*, pp. 2414–2423, 2016.
- Xiangming Gu, Chao Du, Tianyu Pang, Chongxuan Li, Min Lin, and Ye Wang. On memorization in diffusion models. *arXiv preprint arXiv:2310.02664*, 2023.
- Amir Hertz, Ron Mokady, Jay Tenenbaum, Kfir Aberman, Yael Pritch, and Daniel Cohen-Or. Prompt-to-prompt image editing with cross attention control. *arXiv preprint arXiv:2208.01626*, 2022.
- Jonathan Ho and Tim Salimans. Classifier-free diffusion guidance. *arXiv preprint arXiv:2207.12598*, 2022.
- Jonathan Ho, Ajay Jain, and Pieter Abbeel. Denoising diffusion probabilistic models. *Advances in neural information processing systems*, 33:6840–6851, 2020.
- Gabriel Ilharco, Marco Tulio Ribeiro, Mitchell Wortsman, Suchin Gururangan, Ludwig Schmidt, Hannaneh Hajishirzi, and Ali Farhadi. Editing models with task arithmetic. *arXiv preprint arXiv:2212.04089*, 2022.
- Justin Johnson, Bharath Hariharan, Laurens Van Der Maaten, Li Fei-Fei, C Lawrence Zitnick, and Ross Girshick. Clevr: A diagnostic dataset for compositional language and elementary visual reasoning. In *Proceedings of the IEEE conference on computer vision and pattern recognition*, pp. 2901–2910, 2017.
- Zahra Kadkhodaie, Florentin Guth, Eero P Simoncelli, and Stéphane Mallat. Generalization in diffusion models arises from geometry-adaptive harmonic representations. *arXiv preprint arXiv:2310.02557*, 2023.
- Mason Kamb and Surya Ganguli. An analytic theory of creativity in convolutional diffusion models. *arXiv preprint arXiv:2412.20292*, 2024.
- Tero Karras, Samuli Laine, and Timo Aila. A style-based generator architecture for generative adversarial networks. In *Proceedings of the IEEE/CVF conference on computer vision and pattern recognition*, pp. 4401–4410, 2019.

- 
- Tero Karras, Miika Aittala, Timo Aila, and Samuli Laine. Elucidating the design space of diffusion-based generative models. *Advances in neural information processing systems*, 35:26565–26577, 2022.
- Tero Karras, Miika Aittala, Jaakko Lehtinen, Janne Hellsten, Timo Aila, and Samuli Laine. Analyzing and improving the training dynamics of diffusion models. In *Proceedings of the IEEE/CVF Conference on Computer Vision and Pattern Recognition*, pp. 24174–24184, 2024.
- Hyunjik Kim and Andriy Mnih. Disentangling by factorising. In *International conference on machine learning*, pp. 2649–2658. PMLR, 2018.
- Dmytro Kotovenko, Artsiom Sanakoyeu, Sabine Lang, and Bjorn Ommer. Content and style disentanglement for artistic style transfer. In *Proceedings of the IEEE/CVF international conference on computer vision*, pp. 4422–4431, 2019.
- Yuheng Li, Haotian Liu, Qingyang Wu, Fangzhou Mu, Jianwei Yang, Jianfeng Gao, Chunyuan Li, and Yong Jae Lee. Gligen: Open-set grounded text-to-image generation. In *Proceedings of the IEEE/CVF conference on computer vision and pattern recognition*, pp. 22511–22521, 2023.
- Nan Liu, Shuang Li, Yilun Du, Antonio Torralba, and Joshua B Tenenbaum. Compositional visual generation with composable diffusion models. In *European Conference on Computer Vision*, pp. 423–439. Springer, 2022.
- Francesco Locatello, Stefan Bauer, Mario Lucic, Gunnar Raetsch, Sylvain Gelly, Bernhard Schölkopf, and Olivier Bachem. Challenging common assumptions in the unsupervised learning of disentangled representations. In *international conference on machine learning*, pp. 4114–4124. PMLR, 2019.
- Artem Lukoianov, Chenyang Yuan, Justin Solomon, and Vincent Sitzmann. Locality in image diffusion models emerges from data statistics. *arXiv preprint arXiv:2509.09672*, 2025.
- Matthew Niedoba, Berend Zwartsenberg, Kevin Murphy, and Frank Wood. Towards a mechanistic explanation of diffusion model generalization. *arXiv preprint arXiv:2411.19339*, 2024.
- Maya Okawa, Ekdeep S Lubana, Robert Dick, and Hidenori Tanaka. Compositional abilities emerge multiplicatively: Exploring diffusion models on a synthetic task. *Advances in Neural Information Processing Systems*, 36, 2024.
- Core Francisco Park, Maya Okawa, Andrew Lee, Ekdeep S Lubana, and Hidenori Tanaka. Emergence of hidden capabilities: Exploring learning dynamics in concept space. *Advances in Neural Information Processing Systems*, 37:84698–84729, 2024.
- Dustin Podell, Zion English, Kyle Lacey, Andreas Blattmann, Tim Dockhorn, Jonas Müller, Joe Penna, and Robin Rombach. Sdxl: Improving latent diffusion models for high-resolution image synthesis. *arXiv preprint arXiv:2307.01952*, 2023.
- Aditya Ramesh, Prafulla Dhariwal, Alex Nichol, Casey Chu, and Mark Chen. Hierarchical text-conditional image generation with clip latents. *arXiv preprint arXiv:2204.06125*, 1(2):3, 2022.
- Robin Rombach, Andreas Blattmann, Dominik Lorenz, Patrick Esser, and Björn Ommer. High-resolution image synthesis with latent diffusion models. In *Proceedings of the IEEE/CVF conference on computer vision and pattern recognition*, pp. 10684–10695, 2022.
- Antonio Sclocchi, Alessandro Favero, and Matthieu Wyart. A phase transition in diffusion models reveals the hierarchical nature of data. *Proceedings of the National Academy of Sciences*, 122(1): e2408799121, 2025.
- Jascha Sohl-Dickstein, Eric Weiss, Niru Maheswaranathan, and Surya Ganguli. Deep unsupervised learning using nonequilibrium thermodynamics. In *International conference on machine learning*, pp. 2256–2265. pmlr, 2015.
- Yang Song and Stefano Ermon. Generative modeling by estimating gradients of the data distribution. *Advances in neural information processing systems*, 32, 2019.

- 
- Yang Song, Jascha Sohl-Dickstein, Diederik P Kingma, Abhishek Kumar, Stefano Ermon, and Ben Poole. Score-based generative modeling through stochastic differential equations. *arXiv preprint arXiv:2011.13456*, 2020. URL <https://arxiv.org/pdf/2011.13456.pdf>.
- Yutao Sun, Li Dong, Barun Patra, Shuming Ma, Shaohan Huang, Alon Benhaim, Vishrav Chaudhary, Xia Song, and Furu Wei. A length-extrapolatable transformer. 2022.
- Binxu Wang and John J Vastola. Diffusion models generate images like painters: an analytical theory of outline first, details later. *arXiv preprint arXiv:2303.02490*, 2023.
- Peng Wang, Huijie Zhang, Zekai Zhang, Siyi Chen, Yi Ma, and Qing Qu. Diffusion models learn low-dimensional distributions via subspace clustering. *arXiv preprint arXiv:2409.02426*, 2024.
- taemin6697 wooyeolbaek, mbaek01. attention-map-diffusers. <https://github.com/wooyeolbaek/attention-map-diffusers>, 2025.
- Jinheng Xie, Yuexiang Li, Yawen Huang, Haozhe Liu, Wentian Zhang, Yefeng Zheng, and Mike Zheng Shou. Boxdiff: Text-to-image synthesis with training-free box-constrained diffusion. In *Proceedings of the IEEE/CVF International Conference on Computer Vision*, pp. 7452–7461, 2023.
- Han Xue, Zhiwu Huang, Qianru Sun, Li Song, and Wenjun Zhang. Freestyle layout-to-image synthesis. In *Proceedings of the IEEE/CVF conference on computer vision and pattern recognition*, pp. 14256–14266, 2023.
- Zhutian Yang, Jiayuan Mao, Yilun Du, Jiajun Wu, Joshua B Tenenbaum, Tomás Lozano-Pérez, and Leslie Pack Kaelbling. Compositional diffusion-based continuous constraint solvers. *arXiv preprint arXiv:2309.00966*, 2023.
- Jinghan Zhang, Junteng Liu, Junxian He, et al. Composing parameter-efficient modules with arithmetic operation. *Advances in Neural Information Processing Systems*, 36:12589–12610, 2023.
- Guangcong Zheng, Xianpan Zhou, Xuwei Li, Zhongang Qi, Ying Shan, and Xi Li. Layoutdiffusion: Controllable diffusion model for layout-to-image generation. In *Proceedings of the IEEE/CVF Conference on Computer Vision and Pattern Recognition*, pp. 22490–22499, 2023.
- Jun-Yan Zhu, Taesung Park, Phillip Isola, and Alexei A Efros. Unpaired image-to-image translation using cycle-consistent adversarial networks. In *Proceedings of the IEEE international conference on computer vision*, pp. 2223–2232, 2017.

---

## A RELATED WORK

**Locality and generalization in diffusion models** Kamb & Ganguli (2024); Niedoba et al. (2024) argue that “creativity” in unconditional and class-conditional models arises from a bias toward learning local denoisers, while Lukoianov et al. (2025) challenge some of the conclusions of Kamb & Ganguli (2024) by arguing that locality arises from statistical properties of the data rather than network inductive bias. Our work builds on the idea of locality by showing that it can also be a mechanism for compositional generalization in conditional models, which none of the previous works addressed. We are agnostic about whether locality arises from data statistics or inductive bias in practice (likely both are at play); our main insight is that compositional generalization can be achieved when the network learns a local – or equivalently, compositional – structure by any means. (Our Experiment 3 suggests that local architectural interventions can promote learning the underlying compositional structure of the data, but this structure can also be learned “naturally” as in Experiment 1.) Note also that Kamb & Ganguli (2024) propose equivariance while Niedoba et al. (2024); Lukoianov et al. (2025) omit or argue against it; in our theory and experiments equivariance is not necessary.

**Generalization of diffusion models** Kadkhodaie et al. (2023) propose shrinkage in a geometry-adaptive harmonic bias as a mechanism for generalization; in the framework of our theory, this can be thought of as a bias toward sparse dependencies in a particular feature-space. Gu et al. (2023) make an experimentally study of potential causes generalization in unconditional and class-conditional settings based on the characteristics of the dataset and choices for training and model. Bertrand et al. (2025) give empirical evidence that for flow models in high-dimensions, generalization arises primarily from network inductive biases rather than noise in the flow-matching loss.

**Learning Dynamics of Composition** An interesting line of work focuses on the learning dynamics of models trained on compositional data. Okawa et al. (2024); Park et al. (2024) demonstrate sudden emergence of compositional generalization in controlled synthetic settings where they test novel combinations of attributes of a single object (e.g. blue square, red triangle  $\rightarrow$  blue triangle?). Sclocchi et al. (2025); Favero et al. (2025) study learning dynamics in hierarchical models, showing that higher-level features take longer to learn.

**Explicit composition of multiple diffusion models** Du & Kaelbling (2024); Liu et al. (2022); Bradley et al. (2025) study *explicit* compositions of multiple diffusion models via linear score combination, demonstrating length-generalization in CLEVR in some cases. Bradley et al. (2025) proposed Projective Composition as a definition of “correct” compositions of multiple models; here we use it to precisely characterize compositionality in a single conditional model.

**Feature-space disentanglement** Despite significant evidence for the existence of disentangled feature spaces (Chen et al., 2018; Kim & Mnih, 2018; Yang et al., 2023; Locatello et al., 2019; Zhang et al., 2023; Ilharco et al., 2022) and diffusion models’ ability to learn them in some cases Karras et al. (2019); Kotovenko et al. (2019); Gatys et al. (2016); Zhu et al. (2017), feature disentanglement in diffusion representations is still not fully understood.

**Layout-to-Image Diffusion Models** Our theory may help to explain the success of layout-to-image methods that use architectural locality priors (Li et al., 2023; Zheng et al., 2023; Cheng et al., 2023; 2024) or inference-time locality constraints (Dahary et al., 2024; Xue et al., 2023; Xie et al., 2023) to improve multi-object generation. Although these works primarily report improved grounding and controllability rather than explicit OOD composition, their interventions can be viewed as approximate causal tests, where increased locality leads to improved multi-object behavior, consistent with our theory and similar to the causal intervention Exp. 3 (Figure 1).

## B PROOF OF LEMMA 1

*Proof.* (Lemma 1) Let  $p$  be the CPC given by

$$p(x|c_{\mathcal{J}}) := p(x_{M_{\mathcal{J}}^{\mathfrak{c}}}| \emptyset) \prod_{j \in \mathcal{J}} p(x_{M_j}|c_j), \quad \forall \mathcal{J} \in \mathcal{J}_{\text{all}}$$

and let  $s$  be the LCS given by

$$\begin{aligned} s^t[x|c_{\mathcal{J}}](i) &:= \nabla \log p^t[x_{N_i^t}|c_{L_i^t(\mathcal{J})}](i), \quad \forall i, \forall t \\ L_i^t(\mathcal{J}) &= \begin{cases} \{j\} \cap \mathcal{J}, & \text{if } i \in M_j \\ \emptyset, & \text{else} \end{cases} \\ N_i^t &= \begin{cases} M_j, & \text{if } i \in M_j \\ M_b, & \text{else,} \end{cases} \quad \text{where } M_b := M_{\mathcal{J}_{\text{all}}^{\mathfrak{c}}}. \end{aligned}$$

We want to show that  $s$  is exactly the score of  $p$ :

$$s^t(x|c_{\mathcal{J}}) = \nabla \log p^t(x|c_{\mathcal{J}}), \quad \forall \mathcal{J}.$$

To see this, we first analyze  $p^t$  at each pixel  $i$ . We begin by noting that if  $p$  has a pixel-space PC structure at time 0 then it has an identical PC structure at all times  $t$  (Bradley et al., 2025) (because adding isotropic Gaussian noise preserves the independence between subsets).

$$\nabla \log p^t(x|c_{\mathcal{J}}) := \nabla \log p^t(x_{M_{\mathcal{J}}^{\mathfrak{c}}}| \emptyset) + \sum_{j \in \mathcal{J}} \nabla \log p^t(x_{M_j}|c_j), \quad \forall \mathcal{J}$$

$$\begin{aligned} \nabla \log p^t(x_{M_j}|c_j)(i) &= 0, \quad \forall i \notin M_j, \quad \text{since } p^t(x_{M_j}) \text{ does not depend on } x_i \\ \implies j \in \mathcal{J}, \quad i \in M_j &\implies \nabla \log p^t(x|c_{\mathcal{J}})(i) = \nabla \log p^t(x_{M_j}|c_j)(i) \\ j \notin \mathcal{J}, \quad i \in M_j &\implies \nabla \log p^t(x|c_{\mathcal{J}})(i) = \nabla \log p^t(x_{M_j}| \emptyset)(i) \\ i \in M_b &\implies \nabla \log p^t(x|c_{\mathcal{J}})(i) = \nabla \log p_b^t(x_{M_b}| \emptyset)(i). \end{aligned}$$

Next we analyze  $s$  at each pixel  $i$ :

$$\begin{aligned} s^t[x|c_{\mathcal{J}}](i) &:= \nabla \log p^t[x_{N_i^t}|c_{L_i^t(\mathcal{J})}](i) \\ j \in \mathcal{J}, \quad i \in M_j &\implies L_i^t(\mathcal{J}) = \{j\}, \quad N_i^t = M_j \implies s^t[x|c_{\mathcal{J}}](i) = \nabla \log p^t(x_{M_j}|c_j)(i) \\ j \notin \mathcal{J}, \quad i \in M_j &\implies L_i^t(\mathcal{J}) = \emptyset, \quad N_i^t = M_j \implies s^t[x|c_{\mathcal{J}}](i) = \nabla \log p^t(x_{M_j}| \emptyset)(i) \\ i \in M_b &\implies L_i^t = \emptyset, \quad M_b \subseteq N_i^t \implies s^t(x|c_{\mathcal{J}})(i) = \nabla \log p_b^t[x_{M_b}| \emptyset](i). \end{aligned}$$

Comparing  $s^t(x|c_{\mathcal{J}})(i)$  and  $\nabla \log p^t(x|c_{\mathcal{J}})(i)$  in each of the three cases, we see that  $s^t[x|c](i) = \nabla \log p^t(x|c)(i)$  for all pixels  $i$ , hence

$$s^t(x|c_{\mathcal{J}}) = \nabla \log p^t(x|c_{\mathcal{J}}), \quad \forall \mathcal{J}. \quad \square$$

## C RELAXATION OF LEMMA 1

In this section we provide a collection of lemmas showing that the score of an approximately CPC distribution is approximately an LCS, and that this approximation becomes more accurate as noise increases. We state all lemmas first and then provide the proofs at the end.

We begin by defining a notion of *approximate* conditional projective composition.

**Definition 3** (Approximate CPC). *We say that a conditional distribution  $p^t(x|c)$  is approximately-CPC with errors  $\{\varepsilon_j, \tilde{\varepsilon}_j, \varepsilon_b\}$  if*

$$\sup_{x_{M_j^{\mathfrak{c}}}} D_{\text{KL}}[p(x_{M_j}|c_{\mathcal{J}}, x_{M_j^{\mathfrak{c}}})|p(x_{M_j}|c_j)] \leq \varepsilon_j, \quad \forall \mathcal{J}, \quad \forall j \in \mathcal{J} \quad (4)$$

$$\sup_{x_{M_j^{\mathfrak{c}}}} D_{\text{KL}}[p(x_{M_j}|c_{\mathcal{J}}, x_{M_j^{\mathfrak{c}}})|p(x_{M_j}| \emptyset)] \leq \tilde{\varepsilon}_j, \quad \forall \mathcal{J}, \quad \forall j \notin \mathcal{J} \quad (5)$$

$$\sup_{x_{M_b^{\mathfrak{c}}}} D_{\text{KL}}[p(x_{M_b}|c_{\mathcal{J}}, x_{M_b^{\mathfrak{c}}})|p(x_{M_b})] \leq \varepsilon_b, \quad \forall \mathcal{J}. \quad (6)$$

The following lemma is relaxation of Lemma 1. It shows that the score of an *approximately-CPC* distribution is *approximately* an LCS.

**Lemma 2** (LCS approximates score of approximate-CPC). *Let  $p^t(x|c)$  be approximately-CPC with errors  $\{\varepsilon_j, \tilde{\varepsilon}_j, \varepsilon_b\}$  per Definition 3. Define a local conditional score  $s$  as in Lemma 1, and let  $\hat{p}$  be the induced distribution s.t.  $s^t(x|c_{\mathcal{J}}) = \nabla \log \hat{p}^t(x|c_{\mathcal{J}})$ . Then*

$$D_{\text{KL}}(p(\cdot|c_{\mathcal{J}})||\hat{p}(\cdot|c_{\mathcal{J}})) \leq \sum_{j \in \mathcal{J}} \varepsilon_j + \sum_{j \notin \mathcal{J}} \tilde{\varepsilon}_j + \varepsilon_b.$$

Further, we can show that the approximation errors in Definition 3 decrease as noise is added: intuitively, an approximately-compositional distribution gets *more compositional* as noise is added.

**Lemma 3.** *Suppose that the supremum of  $\sup_y [KL(N_t[p](x)||N_t[p](x|y))]$  is attained for all  $t$ . Then*

$$\sup_y [KL(N_t[p](x)||N_t[p](x|y))]$$

*is decreasing in  $t$ .*

The proof of Lemma 3 essentially follows from the fact that adding Gaussian noise decreases the KL divergence between distributions:

**Claim 1** (Standard; KL divergence decreases with noise).

$$\frac{\partial}{\partial t} D_{\text{KL}}(N_t[q]||N_t[r]) = -t \left[ \left( \nabla \log \frac{N_t[q]}{N_t[r]} \right)^2 \right] < 0, \quad \text{if } q \neq r.$$

This is a standard fact but a proof is offered for the reader’s convenience at the end of this section. Note that the Data Processing Inequality immediately implies that the KL divergence is non-increasing, but the claim is that it is actually decreasing.

Combining Lemma 2 and Lemma 3, we see that at high noise levels, distributions become *more compositional*, and thus better-approximated by local-conditional-scores. We now provide the proofs.

*Proof.* (Lemma 2)

Define the “ideal” projective composition for any  $\mathcal{J}$  by:

$$\mathcal{C}_{\mathcal{J}}^*[p](x) := p(x_{M_{\mathcal{J}}^c} | \emptyset) \prod_{j \in \mathcal{J}} p(x_{M_j} | c_j).$$

By Lemma 1, we have that  $s$  is exact for  $\nabla \log \mathcal{C}_{\mathcal{J}}^*[p]$ , and so  $\hat{p}(\cdot|c_{\mathcal{J}}) = \mathcal{C}_{\mathcal{J}}^*[p]$ .

Thus we need to show that

$$D_{\text{KL}}(p(\cdot|c_{\mathcal{J}})||\mathcal{C}_{\mathcal{J}}^*[p]) \leq \sum_{j \in \mathcal{J}} \varepsilon_j + \sum_{j \notin \mathcal{J}} \tilde{\varepsilon}_j + \varepsilon_b.$$

This is essentially a bound on a mean field approximation. First, note that for any  $c$ , we can rewrite  $p(x|c)$  using the chain rule as

$$p(x|c) = p(x_{M_b} | c_{\mathcal{J}}) \prod_{j \in \mathcal{J}_{\text{all}}} p(x_{M_j} | c, x_{M_b}, x_{M_1}, \dots, x_{M_{j-1}})$$

Then calculate

$$\begin{aligned}
D_{\text{KL}}(p(\cdot|c_{\mathcal{J}})||\mathcal{C}_{\mathcal{J}}^*[p]) &\equiv \mathbb{E}_{p(x|c_{\mathcal{J}})} \left[ \log \frac{p(x|c_{\mathcal{J}})}{\mathcal{C}_{\mathcal{J}}^*[p](x)} \right] \\
&= \mathbb{E}_{p(x|c_{\mathcal{J}})} \left[ \log \frac{p(x_{M_b}|c_{\mathcal{J}}) \prod_j p(x_{M_j}|c_{\mathcal{J}}, x_{M_b}, x_{M_1}, \dots, x_{M_{j-1}})}{p(x_{M_b}) \prod_{j \notin \mathcal{J}} p(x_{M_j}|\emptyset) \prod_{j \in \mathcal{J}} p(x_{M_j}|c_j)} \right] \\
&= \sum_{j \in \mathcal{J}} \mathbb{E}_{p(x|c_{\mathcal{J}})} \left[ \log \frac{p(x_{M_j}|c_{\mathcal{J}}, x_{M_b}, x_{M_1}, \dots, x_{M_{j-1}})}{p(x_{M_j}|c_j)} \right] \\
&\quad + \sum_{j \notin \mathcal{J}} \mathbb{E}_{p(x|c_{\mathcal{J}})} \left[ \log \frac{p(x_{M_j}|c_{\mathcal{J}}, x_{M_b}, x_{M_1}, \dots, x_{M_{j-1}})}{p(x_{M_j}|\emptyset)} \right] \\
&\quad + \mathbb{E}_p \left[ \log \frac{p(x_{M_b}|c_{\mathcal{J}})}{p(x_{M_b})} \right] \\
&= \sum_{j \in \mathcal{J}} \mathbb{E}_{p(x_{M_b}, x_{M_1}, \dots, x_{M_{j-1}}|c_{\mathcal{J}})} [D_{\text{KL}}[p(x_{M_j}|c_{\mathcal{J}}, x_{M_b}, x_{M_1}, \dots, x_{M_{j-1}})||p(x_{M_j}|c_j)]] \\
&\quad + \sum_{j \notin \mathcal{J}} \mathbb{E}_{p(x_{M_b}, x_{M_1}, \dots, x_{M_{j-1}}|c_{\mathcal{J}})} [D_{\text{KL}}[p(x_{M_j}|c_{\mathcal{J}}, x_{M_b}, x_{M_1}, \dots, x_{M_{j-1}})||p(x_{M_j}|\emptyset)]] \\
&\quad + \mathbb{E}_{p(x_{M_b}|\mathfrak{c}_{\mathcal{J}})} [D_{\text{KL}}[p(x_{M_b}|c_{\mathcal{J}})||p(x_{M_b})]] \\
&\leq \sum_{j \in \mathcal{J}} \sup_{x_{M_j}^{\mathfrak{c}_{\mathcal{J}}}} D_{\text{KL}}[p(x_{M_j}|c_{\mathcal{J}}, x_{M_j}^{\mathfrak{c}_{\mathcal{J}}})||p(x_{M_j}|c_j)] \\
&\quad + \sum_{j \notin \mathcal{J}} \sup_{x_{M_j}^{\mathfrak{c}_{\mathcal{J}}}} D_{\text{KL}}[p(x_{M_j}|c_{\mathcal{J}}, x_{M_j}^{\mathfrak{c}_{\mathcal{J}}})||p(x_{M_j}|\emptyset)] \\
&\quad + \sup_{x_{M_b}^{\mathfrak{c}_{\mathcal{J}}}} D_{\text{KL}}[p(x_{M_b}|c_{\mathcal{J}}, x_{M_b}^{\mathfrak{c}_{\mathcal{J}}})||p(x_{M_b})] \\
&\leq \sum_{j \in \mathcal{J}} \varepsilon_j + \sum_{j \notin \mathcal{J}} \tilde{\varepsilon}_j + \varepsilon_b
\end{aligned}$$

□

*Proof.* (Lemma 3)

We want to show that

$$t_2 \geq t_1 \implies \sup_y [KL(N_{t_2}[p](x)||N_{t_2}[p](x|y))] < \sup_y [KL(N_{t_1}[p](x)||N_{t_1}[p](x|y))]$$

Let  $t_2 \geq t_1$ . By assumption, the supremum of  $\sup_y [KL(N_{t_2}[p](x)||N_{t_2}[p](x|y))]$  is attained, so let  $y_2^*$  be a value of  $y$  that achieves the supremum for  $t_2$ . Then

$$\begin{aligned}
y_2^* &:= \arg \max_y [KL(N_{t_2}[p](x)||N_{t_2}[p](x|y))] \\
\sup_y [KL(N_{t_1}[p](x)||N_{t_1}[p](x|y))] &:= KL(N_{t_2}[p](x)||N_{t_2}[p](x|y_2^*)) \\
&\leq KL(N_{t_1}[p](x)||N_{t_1}[p](x|y_2^*)), \quad \text{by Claim 1} \\
&\leq \sup_y [KL(N_{t_1}[p](x)||N_{t_1}[p](x|y))]
\end{aligned}$$

□

*Proof.* (Claim 1) We want to show that

$$\frac{\partial}{\partial t} D_{\text{KL}}(N_t[q]||N_t[r]) = -t \left[ \left( \nabla \log \frac{N_t[q]}{N_t[r]} \right)^2 \right] < 0, \quad \text{if } q \neq r.$$

This is a standard result but we provide a proof for the reader's convenience.

$$\begin{aligned}
D_{\text{KL}}(q||r) &:= \mathbb{E}_q[\log \frac{q}{r}] = \int q(x) \log \frac{q(x)}{r(x)} dx \\
N_t[p](x) &:= \int p(y) \mathcal{N}(x; y, t^2) dy \\
\mathbb{E}_{N_t[q]}[\log \frac{N_t[q]}{N_t[r]}] &= \int N_t[q](x) \log \frac{N_t[q](x)}{N_t[r](x)} dx \\
\frac{\partial}{\partial t} \mathbb{E}_{N_t[q]}[\log \frac{N_t[q]}{N_t[r]}] &= \frac{\partial}{\partial t} \int N_t[q](x) \log \frac{N_t[q](x)}{N_t[r](x)} dx \\
&= \int \frac{\partial}{\partial t} N_t[q](x) \cdot \log \frac{N_t[q](x)}{N_t[r](x)} dx + \int N_t[q](x) \cdot \frac{\partial}{\partial t} \log \frac{N_t[q](x)}{N_t[r](x)} dx \\
&\equiv I_1 + I_2
\end{aligned}$$

To work on integrals  $I_1, I_2$ , we use the following fact:  $\frac{\partial}{\partial t} N_t[p](x) = t \nabla^2 N_t[p](x)$  (Equation (7)).

$$\begin{aligned}
I_1 &\equiv \int \frac{\partial}{\partial t} N_t[q](x) \cdot \log \frac{N_t[q](x)}{N_t[r](x)} dx \\
&= \int t \nabla^2 N_t[q](x) \cdot \log \frac{N_t[q](x)}{N_t[r](x)} dx, \quad \text{using } \frac{\partial}{\partial t} N_t[p] = t \nabla^2 N_t[p] \text{ as shown below} \\
&= -t \int \nabla N_t[q](x) \cdot \nabla \log \frac{N_t[q](x)}{N_t[r](x)} dx, \quad \text{integration by parts} \\
&= -t \int \nabla N_t[q](x) \cdot (\nabla \log N_t[q](x) - \nabla \log N_t[r](x)) dx, \\
&= -t \int \nabla N_t[q] \cdot \left( \frac{\nabla N_t[q]}{N_t[q]} - \frac{\nabla N_t[r]}{N_t[r]} \right) dx \\
&= t \int -\frac{\nabla N_t[q]^2}{N_t[q]} + \frac{\nabla N_t[r] \nabla N_t[q]}{N_t[r]} dx
\end{aligned}$$

$$\begin{aligned}
I_2 &\equiv \int N_t[q](x) \cdot \frac{\partial}{\partial t} \log \frac{N_t[q](x)}{N_t[r](x)} dx \\
\frac{\partial}{\partial t} \log \frac{N_t[q](x)}{N_t[r](x)} &= \frac{\partial}{\partial t} \log N_t[q](x) - \frac{\partial}{\partial t} \log N_t[r](x) \\
&= \frac{1}{N_t[q](x)} \frac{\partial}{\partial t} N_t[q](x) - \frac{1}{N_t[r](x)} \frac{\partial}{\partial t} N_t[r](x) \\
&= \frac{t}{N_t[q](x)} \nabla^2 N_t[q](x) - \frac{t}{N_t[r](x)} \nabla^2 N_t[r](x) \\
\implies I_2 &= t \int N_t[q](x) \cdot \left( \frac{\nabla^2 N_t[q](x)}{N_t[q](x)} - \frac{\nabla^2 N_t[r](x)}{N_t[r](x)} \right) dx \\
&= -t \int \frac{N_t[q](x)}{N_t[r](x)} \nabla^2 N_t[r] dx, \quad \text{since } \int \nabla^2 N_t[q] dx = \nabla N_t[q]|_{-\infty}^{\infty} = 0 \\
&= t \int \nabla \left( \frac{N_t[q](x)}{N_t[r](x)} \right) \nabla N_t[r] dx, \quad \text{integration by parts} \\
&= t \int \frac{\nabla N_t[r] \nabla N_t[q]}{N_t[r]} - \frac{\nabla N_t[r]^2 N_t[q]}{N_t[r]^2} dx
\end{aligned}$$

Therefore

$$\begin{aligned}
I_1 + I_2 &= t \int -\frac{\nabla N_t[q]^2}{N_t[q]} + \frac{\nabla N_t[r] \nabla N_t[q]}{N_t[r]} dx + t \int \frac{\nabla N_t[r] \nabla N_t[q]}{N_t[r]} - \frac{\nabla N_t[r]^2 N_t[q]}{N_t[r]^2} dx \\
&= -t \int \frac{\nabla N_t[q]^2}{N_t[q]} - 2 \frac{\nabla N_t[r] \nabla N_t[q]}{N_t[r]} + \frac{\nabla N_t[r]^2 N_t[q]}{N_t[r]^2} dx \\
&= -t \int N_t[q] \left( \frac{\nabla N_t[q]}{N_t[q]} - \frac{\nabla N_t[r]}{N_t[r]} \right)^2 dx \\
&= -t \left[ \left( \nabla \log \frac{N_t[q]}{N_t[r]} \right)^2 \right]
\end{aligned}$$

This concludes the proof. Note that the fact used earlier can be shown as follows:

$$\text{Claim: } \frac{\partial}{\partial t} N_t[p](x) = t \nabla^2 N_t[p](x) \quad (7)$$

To see this:

$$\begin{aligned}
N_t[p](x) &:= \int p(y) \phi(y) dy, \quad \phi(y; x, t) := \frac{1}{\sqrt{2\pi t^2}} e^{-\frac{(x-y)^2}{2t^2}} \\
\frac{\partial}{\partial t} \phi(y; x, t) &= \frac{1}{\sqrt{2\pi}} \left[ -\frac{1}{t^2} + \frac{(x-y)^2}{t^4} \right] e^{-\frac{(x-y)^2}{2t^2}} = \left[ \frac{(x-y)^2}{t^3} - \frac{1}{t} \right] \phi(y; x, t) \\
\frac{\partial^2}{\partial x^2} \phi(y; x, t) &= \frac{1}{\sqrt{2\pi t^2}} \left[ \frac{(x-y)^2 - t^2}{t^4} \right] e^{-\frac{(x-y)^2}{2t^2}} = \frac{1}{t} \left[ \frac{(x-y)^2}{t^3} - \frac{1}{t} \right] \phi(y; x, t) \\
\implies \frac{\partial}{\partial t} N_t[p](x) &= \int p(y) \frac{\partial}{\partial t} \phi(y; x, t) dy = \int p(y) \left[ \frac{(x-y)^2}{t^3} - \frac{1}{t} \right] \phi(y; x, t) dy \\
\nabla^2 N_t[p](x) &= \int p(y) \frac{\partial^2}{\partial x^2} \phi(y; x, t) dy = \int p(y) \frac{1}{t} \left[ \frac{(x-y)^2}{t^3} - \frac{1}{t} \right] \phi(y; x, t) dy \\
\implies t \nabla^2 N_t[p](x) &= \frac{\partial}{\partial t} N_t[p](x)
\end{aligned}$$

□

## D FEATURE-SPACE THEORY

In this section we discuss the relationship between CPC and LCS in feature space. Inspired by the feature-space adaptation of PC in Bradley et al. (2025), we define feature-space conditional projective composition as follows:

**Definition 4** (Feature-space Conditional Projective Composition (F-CPC)). *We say that  $p(x|c)$  is a F-CPC under an invertible transform  $\mathcal{A} : \mathbb{R}^n \rightarrow \mathbb{R}^n$  (mapping pixel-space to feature-space), if  $\mathcal{A}\sharp p$  (where  $\sharp$  denotes the pushforward) is a CPC according to Definition 2, that is: there exist disjoint sets  $M_j$  for all conditions  $j \in \mathcal{J}_{all}$  such that, for any set of conditions  $\mathcal{J} \in \mathcal{J}_{all}$ ,*

$$(\mathcal{A}\sharp p)(z|c_{\mathcal{J}}) := (\mathcal{A}\sharp p)(z_{M_{\mathcal{G}}}|\emptyset) \prod_{j \in \mathcal{J}} (\mathcal{A}\sharp p)(z_{M_j}|c_j), \quad \text{where } z := \mathcal{A}(x). \quad (8)$$

That is,  $p$  is an F-CPC if it has CPC compositional structure under an appropriate feature-space mapping. In order to exploit this sparse dependency structure, the model now needs to learn the associated feature-space transform and its inverse, in addition to the local subsets  $N_i, L_i$ . For F-CPC distributions, Corollary 1 follows directly from Lemma 1. We formally restate and prove Corollary 1:

**Corollary 1** (LCS is exact for CPC in feature-space; formal). *Suppose that  $p(x|c)$  is an F-CPC (Definition 4) under an invertible transform  $\mathcal{A} : \mathbb{R}^n \rightarrow \mathbb{R}^n$ , with subsets  $\{M_j : j \in \mathcal{J}_{all}\}$ . Letting  $z := \mathcal{A}(x)$  consider the specific local-conditional score  $s$  given by*

$$s_{\mathcal{A}}^t[z|c_{\mathcal{J}}](i) := \nabla_z \log(\mathcal{A}\sharp p)^t[z_{N_i^t}|c_{L_i^t(\mathcal{J})}](i),$$

where  $N_i, L_i$  are defined as in Lemma 1 w.r.t. the subsets  $\{M_j\}$ . Then  $s_{\mathcal{A}}^t[z|c_{\mathcal{J}}]$  is exact for the score of  $\mathcal{A}\sharp p(z|c_{\mathcal{J}})$  w.r.t.  $z$ :

$$s_{\mathcal{A}}^t(z|c_{\mathcal{J}}) = \nabla_z \log(\mathcal{A}\sharp p)^t(z|c_{\mathcal{J}}), \quad \forall \mathcal{J}.$$

*Proof.* Apply Lemma 1 to  $\mathcal{A}\sharp p(z|c)$ . □

Sampling with this local score is more complex than it looks, however! As discussed in Bradley et al. (2025), since the noising operator does not commute with  $\mathcal{A}$ , that is,  $(\mathcal{A}\sharp p)^t \neq \mathcal{A}\sharp(p^t)$ , sampling from  $p$  using  $s_{\mathcal{A}}^t$  would actually requires the process

$$N_t[p] \xrightarrow{\mathcal{A}^t} N_t[\mathcal{A}\sharp p] \xrightarrow{s_{\mathcal{A}}^t} N_{t-1}[\mathcal{A}\sharp p] \xrightarrow{(\mathcal{A}^{t-1})^{-1}} N_{t-1}[p] \rightarrow \dots \rightarrow p,$$

where  $N_t$  denotes the noising operator, i.e.  $N_t[p] := p^t$ , and  $\mathcal{A}^t$  corrects for the non-commutativity:

$$\mathcal{A}^t \sharp N_t[p] := N_t[\mathcal{A}\sharp p].$$

Therefore, it is not enough to learn a single transform  $\mathcal{A}$  and its inverse  $\mathcal{A}^{-1}$  – the network actually needs to learn a time-dependent transform/inverse pair  $\mathcal{A}^t, \mathcal{A}^{-1}$  accounting for the interaction between  $\mathcal{A}$  and the noising process at each time  $t$ , which actually depends on the (unknown) distribution  $p$ . How feasible this is is currently unclear.

However, there are a few special-case worth noting. First, if  $\mathcal{A}$  is an orthogonal transform then we have  $\mathcal{A}^t = \mathcal{A}$  for all  $t$ . Second, we can show that as the noise level increases, the non-commutativity becomes less severe:

**Claim 2.**

$$\frac{\partial}{\partial t} D_{\text{KL}}(N_t[\mathcal{A}\sharp p] || \mathcal{A}\sharp N_t[p]) < 0.$$

Thus, if the composition structure is most important for resolving global structure at high noise levels, it may be enough to learn the single transform  $\mathcal{A}$  in order to approximately exploit the compositional structure.

*Proof.* (Claim 2) We want to show that

$$\frac{\partial}{\partial t} D_{\text{KL}}(N_t[\mathcal{A}\sharp p] || \mathcal{A}\sharp N_t[p]) < 0.$$

$$\begin{aligned} \frac{\partial}{\partial t} D_{\text{KL}}(N_t[\mathcal{A}\sharp p] || \mathcal{A}\sharp N_t[p]) &= \frac{\partial}{\partial t} \int N_t[\mathcal{A}\sharp p] \log \frac{N_t[\mathcal{A}\sharp p]}{\mathcal{A}\sharp N_t[p]} \\ &= \int \frac{\partial}{\partial t} N_t[\mathcal{A}\sharp p] \cdot \log \frac{N_t[\mathcal{A}\sharp p]}{\mathcal{A}\sharp N_t[p]} + \int N_t[\mathcal{A}\sharp p] \cdot \frac{\partial}{\partial t} \log \frac{N_t[\mathcal{A}\sharp p]}{\mathcal{A}\sharp N_t[p]} \\ &:= I_1 + I_2 \end{aligned}$$

$$\begin{aligned} I_1 &:= \int \frac{\partial}{\partial t} N_t[\mathcal{A}\sharp p] \cdot \log \frac{N_t[\mathcal{A}\sharp p]}{\mathcal{A}\sharp N_t[p]} \\ &= t \int \nabla^2 N_t[\mathcal{A}\sharp p] \cdot \log \frac{N_t[\mathcal{A}\sharp p]}{\mathcal{A}\sharp N_t[p]} \\ &= -t \int \nabla N_t[\mathcal{A}\sharp p] \cdot \nabla \log \frac{N_t[\mathcal{A}\sharp p]}{\mathcal{A}\sharp N_t[p]} \\ &= t \int -\frac{\nabla N_t[\mathcal{A}\sharp p]^2}{N_t[\mathcal{A}\sharp p]} + \frac{\nabla N_t[\mathcal{A}\sharp p] \nabla \mathcal{A}\sharp N_t[p]}{\mathcal{A}\sharp N_t[p]} \end{aligned}$$

$$\begin{aligned}
I_2 &= \int N_t[\mathcal{A}\#p] \cdot \frac{\partial}{\partial t} \log \frac{N_t[\mathcal{A}\#p]}{\mathcal{A}\#N_t[p]} \\
&= \int N_t[\mathcal{A}\#p] \cdot \left( \frac{\frac{\partial}{\partial t} N_t[\mathcal{A}\#p]}{N_t[\mathcal{A}\#p]} - \frac{\frac{\partial}{\partial t} \mathcal{A}\#N_t[p]}{\mathcal{A}\#N_t[p]} \right) \\
&= t \int N_t[\mathcal{A}\#p] \cdot \left( \frac{\nabla^2 N_t[\mathcal{A}\#p]}{N_t[\mathcal{A}\#p]} - \frac{\nabla^2 \mathcal{A}\#N_t[p]}{\mathcal{A}\#N_t[p]} \right) \\
&= t \int \nabla^2 N_t[\mathcal{A}\#p] - \frac{N_t[\mathcal{A}\#p]}{\mathcal{A}\#N_t[p]} \nabla^2 \mathcal{A}\#N_t[p] \\
&= -t \int \frac{N_t[\mathcal{A}\#p]}{\mathcal{A}\#N_t[p]} \nabla^2 \mathcal{A}\#N_t[p], \quad \text{since } \int \nabla^2 N_t[\mathcal{A}\#p] = \nabla N_t[\mathcal{A}\#p]|_{-\infty}^{\infty} = 0 \\
&= t \int \nabla \left( \frac{N_t[\mathcal{A}\#p]}{\mathcal{A}\#N_t[p]} \right) \nabla \mathcal{A}\#N_t[p] \\
&= t \int \frac{\nabla N_t[\mathcal{A}\#p] \nabla \mathcal{A}\#N_t[p]}{\mathcal{A}\#N_t[p]} - \frac{N_t[\mathcal{A}\#p] \nabla \mathcal{A}\#N_t[p]^2}{\mathcal{A}\#N_t[p]^2}
\end{aligned}$$

$$\begin{aligned}
\frac{\partial}{\partial t} D_{\text{KL}}(N_t[\mathcal{A}\#p] || \mathcal{A}\#N_t[p]) &= I_1 + I_2 \\
&= -t \int \frac{\nabla N_t[\mathcal{A}\#p]^2}{N_t[\mathcal{A}\#p]} - 2 \frac{\nabla N_t[\mathcal{A}\#p] \nabla \mathcal{A}\#N_t[p]}{\mathcal{A}\#N_t[p]} + \frac{N_t[\mathcal{A}\#p] \nabla \mathcal{A}\#N_t[p]^2}{\mathcal{A}\#N_t[p]^2} \\
&= -t \int N_t[\mathcal{A}\#p] \left( \frac{\nabla N_t[\mathcal{A}\#p]}{N_t[\mathcal{A}\#p]} - \frac{\nabla \mathcal{A}\#N_t[p]}{\mathcal{A}\#N_t[p]} \right)^2 dx \\
&= -t \mathbb{E}_{N_t[\mathcal{A}\#p]} \left[ \left( \nabla \log \frac{N_t[\mathcal{A}\#p]}{\mathcal{A}\#N_t[p]} \right)^2 \right] < 0
\end{aligned}$$

□

## E CLEVR: DETAILS AND ADDITIONAL EXPERIMENTS

### E.1 CLEVR DATASET, ARCHITECTURE, AND TRAINING DETAILS

We used the CLEVR Johnson et al. (2017) dataset generation procedure<sup>3</sup> to generate customized datasets. All default objects, shapes, sizes, colors were kept unchanged. Images were generated in their original resolution of  $320 \times 240$  and down-sampled to a lower resolution of  $128 \times 128$ . We generated various datasets with 1 to  $K$  objects, with 500,000 samples for each object count, for  $K = 1, \dots, 6$ . For example, for models trained on 1-3 objects there are a total of 1,500,000 samples, with 500,000 each for each object count 1, 2, or 3. Note that objects can interact with each other in this dataset: potentially occluding or casting shadows on each other.

Our experiments cover two different conditioning setups. Location-conditioning conditions on 2D object locations, implemented as an 2D integer array representing a `grid_size`  $\times$  `grid_size` grid over the image recording the count of objects whose center falls within the grid cell, as shown in Figure 9. The count is usually zero or 1 but can be greater than 1 if object centers happen to land within the same grid cell. We take `grid_size=16` in all experiments. We either record the locations of all objects, or just one of the objects (randomly selected), in the conditioning grid, depending on the experiment. Color conditioning is implemented as a 8-dimensional integer array (there are 8 possible colors) indicating the count of objects with the corresponding color. In all experiments we condition only a single attribute (either location or color) at a time, with all other attributes sampled randomly and not conditioned on.

<sup>3</sup><https://github.com/facebookresearch/clevr-dataset-gen>

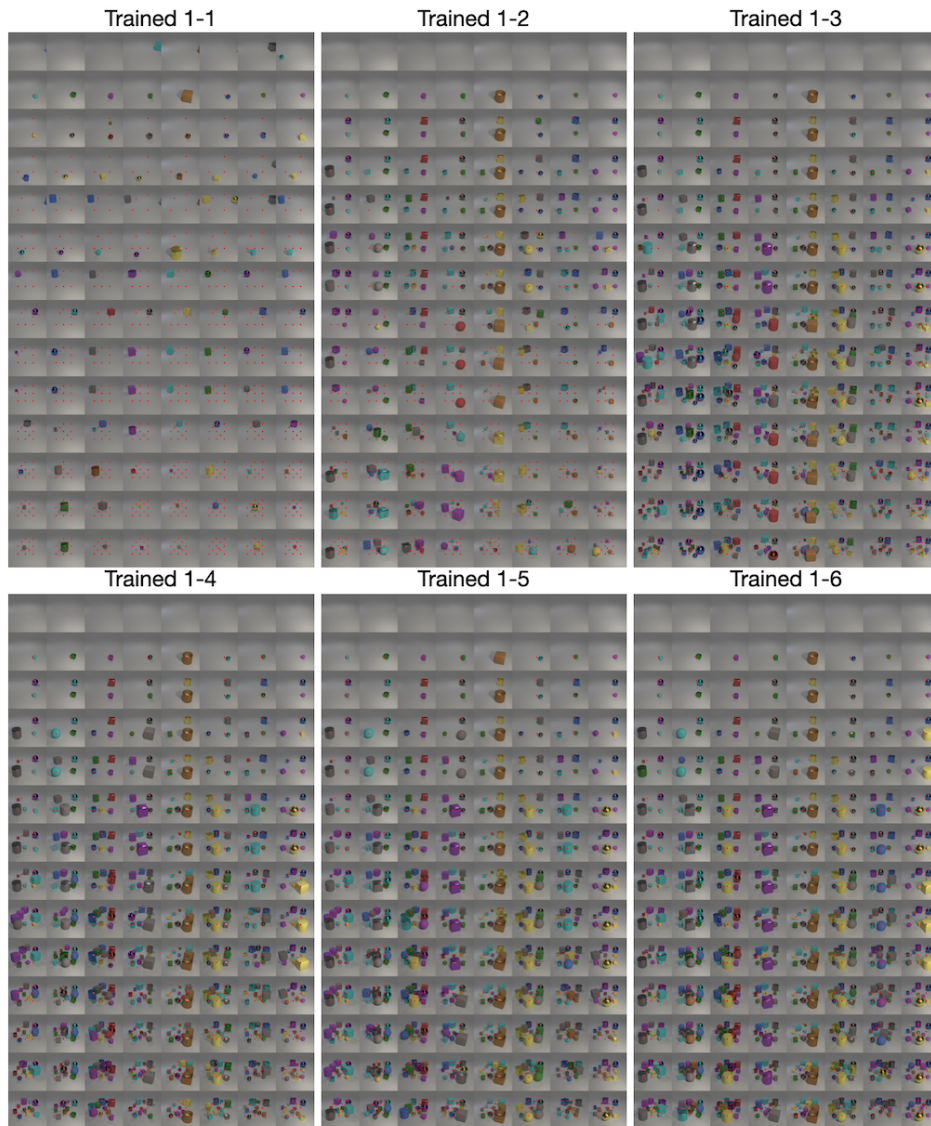


Figure 8: **Length-generalization in Experiment 1 model trained on  $1 - M$  objects.** We tested length-generalization from  $K = 0$  to  $K = 12$  conditioned locations in each model (each row shows 8 samples for a particular  $K$ ).

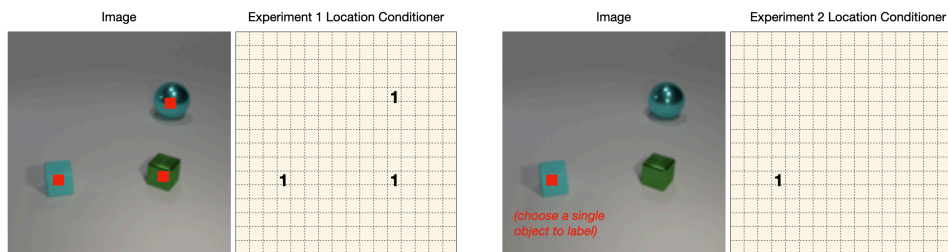


Figure 9: Examples of location conditioning used in Experiments 1, 2, 3 in Figure 1.

Table 2: Learned compositions limits of length-generalization. In the top table we give the maximum value,  $K_{\max}$ , such that the model “succeeds” for every  $1 \leq K \leq K_{\max}$ . In the bottom table, we test  $K = 0$  (which is also OOD) and give the range of the number of objects typically produced. Configurations not tested are left blank. Parentheses indicate extra objects at non-conditioned locations, e.g. +(0-2) means there were 0 to 2 extra objects in addition to the  $K$  at specified locations. All models are location-conditioned but with different variants: All labels means every object was labeled (Experiment 1), Single label means only one object (randomly selected) was labeled (Experiment 2), Rand num labels means a random number of objects were labeled, and Drop one label means all but one object (randomly selected) were labeled.

Train data	All labels	Single label	Rand num labels	Drop one label
1 object	1			
1-2 objects	5	1 +(0-1)	3	
1-3 objects	9	1 +(0-2)	5	3 +(0-1)
1-4 objects	10	1 +(0-3)	6	8 +(0-1)
1-5 objects	10	1 +(0-4)	8	9 +(0-1)
1-6 objects	11	1 +(0-5)	9	10 +(0-1)
Train data	All labels	Single label	Rand num labels	Drop one label
1 objects	0-1			
1-2 objects	0	0-2	0-1	
1-3 objects	0	0-3	0-3	0-1
1-4 objects	0	1-4	0-4	0-1
1-5 objects	0	0-5	0-4	0-1
1-6 objects	0	1-6	0-4	0-1

The 12 locations used for the location-conditioned CLEVR experiments are

```
locations = ([[0.65, 0.65], [0.65, 0.25], [0.25, 0.65], [0.35, 0.35],
[0.45, 0.65], [0.45, 0.25], [0.65, 0.45], [0.25, 0.45],
[0.45, 0.45], [0.55, 0.55], [0.35, 0.55], [0.55, 0.35]]),
```

and the colors are

```
colors = ([blue, brown, cyan, gray, green, purple, red, yellow]).
```

We used our own functionally equivalent re-implementation of the EDM2 Karras et al. (2024) U-net architecture. We used the smallest model architecture, e.g. edm2-img64-xs from <https://github.com/NVlabs/edm2>. This model has a base channel width of 128, resulting in a total of 124M trainable weights.

In all experiments, the model is trained with a batch size of 2048 over  $128 \times 2^{20}$  samples by looping over the dataset as often as needed to reach that number. We use almost the same training procedure as in EDM2 Karras et al. (2024) (the only difference is that we do weight renormalization after the weights are updated). At inference, we use raw conditional diffusion scores, without applying any guidance/CFG (Ho & Salimans, 2022).

## E.2 LENGTH GENERALIZATION EVALUATION

In Table 1, we define  $K_{\max}$  as the maximum value such that the model “succeeds” for every  $1 \leq K \leq K_{\max}$ , with “success” defined for  $1 \leq K \leq N$  as generating exactly  $K$  objects, and (rather generously) for  $K > N$  as generating at least  $K - 2$  and  $K$  objects more than 25% of the time, with objects appearing in approximately correct locations and with acceptable image quality. To assess these criteria, we manually counted over 8 samples of each composition. We tested on up to  $K = 12$  locations and up to  $K = 8$  colors. Table 2 provides a similar analysis for additional experiments with other labeling configurations such as labeling a random number of objects.

In Table 1 and Figure 8 we observe improvements in length-generalization as we increase the maximum number  $M$  of objects the model was trained on, for models that length-generalize at all (i.e. Experiments 1 and 3). We note that for larger numbers of locations  $K$  at inference-time, the objects

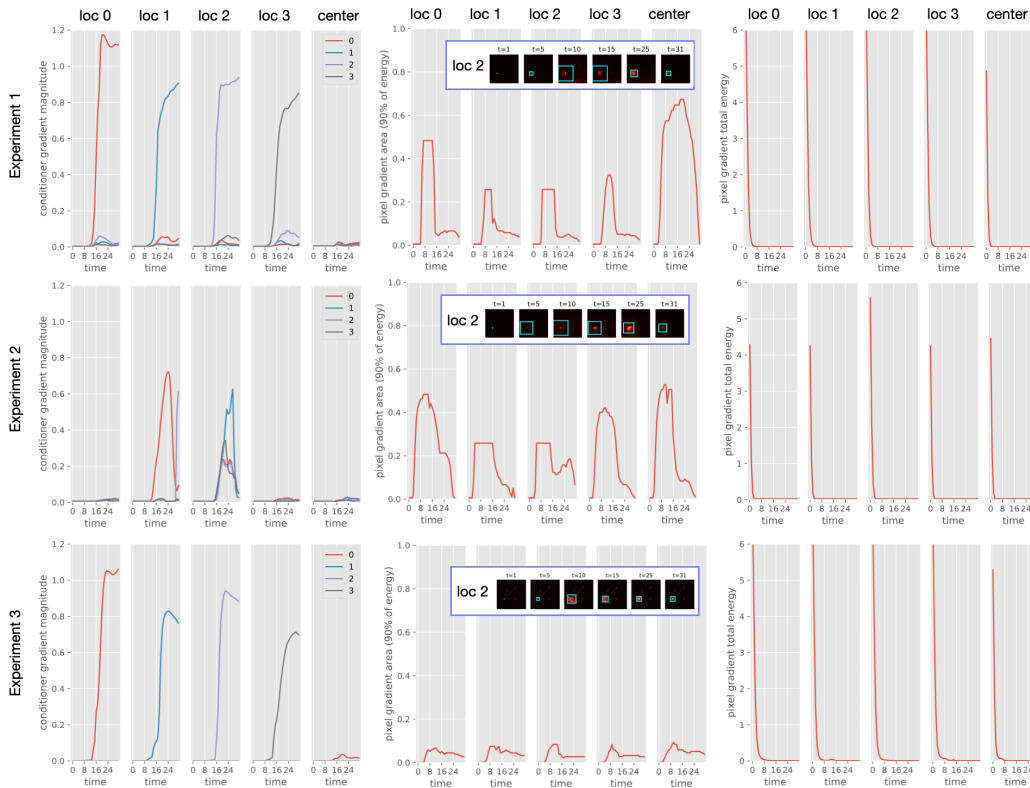


Figure 10: **Locality metrics for CLEVR length generalization** for Experiments 1, 2, and 3, conditioned OOD on 4 locations, as in Figure 2. (Left) Conditioner gradient magnitudes at selected pixel probes (loc 0–3 and center), with colors indicated individual conditioners. Experiment 1 shows strong conditional-locality at high noise (each probe responds only to its corresponding conditioner), whereas Experiment 2 exhibits weaker, non-local responses. Experiment 3 has conditional-locality explicitly enforced by the architecture. (Middle) Pixel gradient area required to cover 90% of score gradient “energy” (sum of squared magnitudes). Insets illustrate the selected square regions at loc 2 at a few timesteps. We observe similar pixel-locality between Experiment 1 and Experiment 2; the pixel gradients are highly localized at both high and low noise, but delocalize during intermediate timesteps. Experiment 3 has pixel-locality explicitly enforced by the architecture. (Right) Total pixel gradient energy (over entire image), which is higher at low noise levels, consistent with conditioners dominating the score field at high noise and pixel interactions emerging later in denoising.

become crowded (less independent). We hypothesize that in general, models trained on  $1 - M$  objects could learn to represent clusters of  $1 - M$  objects, as well as how to compose multiple clusters. (This is still consistent with our theory: it is a conditional projective composition where the conditioners are *subsets*. If the underlying data has this type of compositional structure, a trained model could learn to group individual conditioners into subsets in order to exploit it.) If this is the case, a model trained on 1-3 objects could generate, for instance, 12 objects, by composing 4 clusters of 3 objects each. This would mean that models trained on more objects (larger  $M$ ) could more easily length-generalize to higher  $K$  where objects become crowded.

### E.3 DETAILS OF EXPERIMENT 3: LOCAL PATCH-BASED ARCHITECTURE INTERVENTION.

For Experiment 3 (Figure 1), we developed a local variant of the EDM2 model that processes images as a grid of overlapping patches. The image is divided into a  $\text{grid\_size} \times \text{grid\_size}$  grid of cells, where each cell has size  $m = \text{resolution} / \text{grid\_size}$ . We set  $\text{grid\_size} = 16$  to match the location-conditioning grid. For each grid cell at position  $(i, j)$ , we extract a patch of size  $M = (2k + 1) \times m$ , where  $k$  is the neighborhood radius. We used  $k = 2$  for the experiments in this paper. Each patch is conditioned only on the location-conditioners that fall within the patch – that

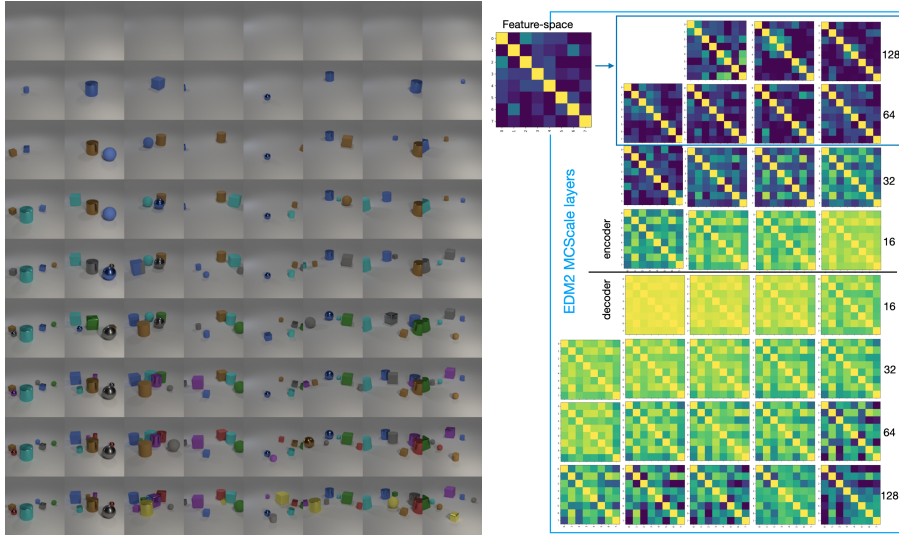


Figure 11: Additional detail for Figure 5 color-conditioned CLEVR study. Complete length-generalization plots (1 to 8 colors;  $> 5$  colors is OOD) and cosine similarities between colors for all EDM2 MCScale layers (both encoder and decoder).

is, a  $(2k + 1) \times (2k + 1)$  subgrid of the full conditioning grid. Each patch is also conditioned on its absolute location (that is, the model is not equivariant). This is implemented by appending the patch center coordinates  $i, j$  to the flattened location-conditioner grid to form the complete conditioner. The training procedure uses a patch sampling approach balancing positive and negative examples for efficiency. For each training image, we randomly sample two patches: one “positive” patch with at least one active conditioner, and one “negative” patch with no active conditioners. Standard EDM2 loss is applied to each patch and losses are averaged.

At inference, we reconstruct the full image by processing each grid cell as follows: extract the corresponding noisy patch and local conditioner; denoise the patch using the trained local model; copy the center region (the single cell) of the denoised patch back to the full image.

In Experiment 3, we trained the local model on the same dataset and location-conditioning (labeling only a single object) as in Exp. 2, showing that Exp. 3 restores length-generalization that failed in Exp. 2. As a test, we also verified that setting  $k = 8$  (which for grid size 16 makes the patches the size of the image) reproduces the behavior of Exp. 2 (i.e. length-generalization fails). We also trained the local model on a dataset with only a single object per image and show that it length-generalizes up to 6 objects in this case, whereas a standard model trained on only one object per image only generates one object per image at test time, regardless of conditioning (Figure 4).

#### E.4 DETAIL OF COLOR-CONDITIONED CLEVR FEATURE-SPACE STUDY.

In Figure 5, the similarity matrices show cosine similarities (heuristic Equation (3)) between network layer activations, when the model is conditioned on different colors (that is, the  $i, j$  entry is the cosine similarity between the mean difference vectors for colors  $i$  and  $j$ ). We perform the study on MCScale layers, which play a similar role to cross-attention in EDM2. Figure 5 shows the encoder MCScale layers only; Figure 11 provides the complete length-generalization plots and cosine similarities between colors for all EDM2 MCScale layers. We identify a possible disentangled feature-space within the early encoder layers: specifically the layers with resolution 128 and 64 (in the figure, the average of these layers is labeled the “feature-space”). Note that this is an empirical and subjective identification, based on our observation that the cosine-similarity heuristic suggests disentanglement within these particular layers; we currently have no theoretical basis for predicting whether and where such disentanglement might occur within the network. Nevertheless, the fact that disentanglement does seem to appear *anywhere* within the network’s internal representation helps to explain the observed partial length generalization according to our theory.

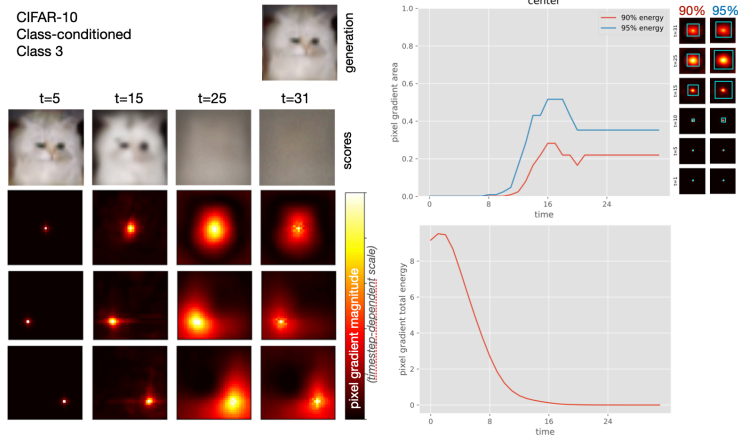


Figure 12: **Pixel locality structure across time for CIFAR-10**, using the same EDM2 architecture from the CLEVR experiments. (Right) Each column represents a timestep  $t$ , and the top row shows the predicted denoised images via learned scores. Lower rows show heatmaps of the pixel gradient magnitude (average absolute Jacobian from an selected pixel to all other pixels). Evaluation at three pixel locations confirms prior empirical observations of Kamb & Ganguli (2024); Niedoba et al. (2024) that the effective local neighborhood size is large at high noise levels. (Left) Locality metrics as in Figure 10; details in Section F.

## F PIXEL- AND CONDITIONAL-LOCALITY GRADIENT ANALYSES

In this section we describe the pixel- and conditional-locality analyses used in Figures 2, 6, 12, 10.

**Pixel Gradient Magnitude** We follow Niedoba et al. (2024) in measuring the average absolute of Jacobian from one pixel to all other pixels. The gradient computation uses automatic differentiation to compute the derivative of each output channel at the target pixel with respect to all input pixels. Specifically, for a model output  $\hat{x}_0 = f_\theta(x_t, t, c)$  with shape  $[B, C, H, W]$ , we compute:

$$G_{i,j}(x, y, t) = \frac{1}{B} \sum_{b=1}^B \sum_{c=1}^3 \left| \frac{\partial \hat{x}_0[b, c, y, x]}{\partial x_t[b, c, i, j]} \right| \quad (9)$$

where  $(x, y)$  is the target pixel and  $(i, j)$  ranges over all input pixels. The spatial gradient map  $G \in \mathbb{R}^{H \times W}$  indicates how strongly each input location influences the prediction at the target pixel.

**Conditional Gradient Magnitude** To measure the influence of each conditioning label on the prediction at a target pixel location, we approximate the “conditional gradient” via a finite difference by computing output differences when individual labels are ablated from the conditioning set.

Given a conditioning set  $C = \{c_1, c_2, \dots, c_K\}$ , we compute the influence of condition  $c_k$  at target pixel  $(x, y)$  as:

$$I_k(x, y, t) = \|f_\theta(x_t, t, C)[x, y] - f_\theta(x_t, t, C_{-k})[x, y]\|_2 \quad (10)$$

where  $C_{-k}$  represents the conditioning set with label  $k$  removed, and the norm is taken across color channels. The method is implemented using forward passes only (no actual gradients are required).

**Locality Metrics** In Figure 10 we directly plot the gradient influence  $I_k(x, y)$  for each conditioner  $k$  across all times  $t$ . We quantify spatial locality by finding the smallest square centered at each target location that contains a specified fraction (90%) of the total gradient energy, i.e. the smallest square  $s$  s.t.  $\sum_{(i,j) \in \text{square}_s} G_{i,j}^2 \geq 0.9 \times \sum_{i,j} G_{i,j}^2$ .

## G SDXL EXPERIMENT DETAILS.

For Figure 6 we use a pretrained SDXL model (out-of-the-box, no finetuning), specifically `stabilityai/stable-diffusion-xl-base-1.0`, with the prompt “a beautiful photo-

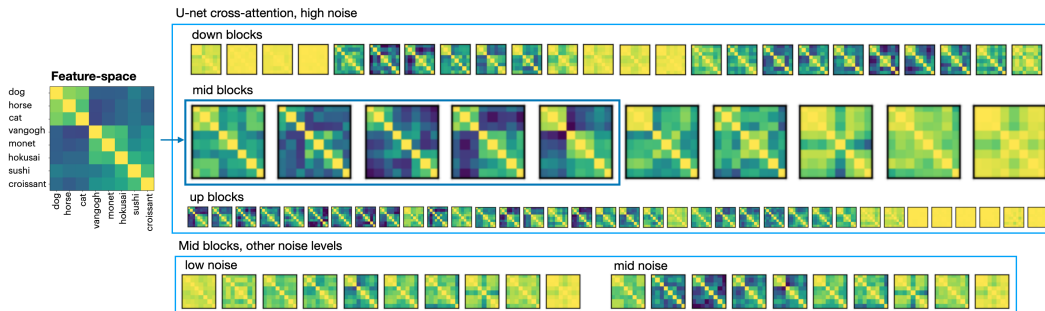


Figure 13: Additional detail for Figure 7. Cosine similarities between selected concepts for all SDXL cross-attention layers. The mid block activations at low and mid noise levels are also shown; note that the disentanglement is weaker at low noise. Disentanglement is most evident in the early mid blocks at high noise, suggesting these layers may serve as a compositional feature-space.

graph with a horse in the middle, a dog on the left, and a cat on the right” – which contains implicit location conditioning. We perform a locality analysis similar to the one we used for CLEVR as described in Section F, but with a few adaptations. The gradient computation is performed in the VAE latent space. Since SDXL uses more complex conditioning, the conditioning influence analysis takes  $C = \{\text{text\_embeds}, \text{pooled\_embeds}, \text{time\_ids}\}$  and  $C_{-k}$  represents the conditioning with word  $k$  removed from the text prompt. Specifically, we first tokenize the input prompt into individual words, remove common words like “a”, “the”, etc., and for each remaining word creating a modified prompt by removing that word. We then compute the score difference w.r.t. the modified prompt. We rank the words by their influence magnitude to study how specific words affect the score at particular pixel locations. We consider a set of words “dominant” if their minimum influence magnitude is at least 2x the influence of the next-ranked word. We ran the model with 50 inference steps using the standard `EulerDiscreteScheduler` stopped at steps  $t = 1, 25, 50$ .

For Figure 7 we used the SDXL model (`stabilityai/stable-diffusion-xl-base-1.0`) as above. We used the following prompts for the feature-space analysis (listed with the shorthand used in the figure):

- dog: “A dog, full body, highly detailed photograph.”
- horse: “A horse, full body, highly detailed photograph.”
- cat: “A cat, full body, highly detailed photograph.”
- vangogh: “An oil-painting in the style of Van Gogh.”
- monet: “A watercolor-painting in the style of Monet.”
- hokusai: “A woodblock print in the style of Hokusai.”
- sushi: “Eating sushi with chopsticks, highly detailed photograph.”
- croissant: “Eating a croissant, highly detailed photograph.”
- vangogh+cat+sushi: “A cat eating sushi with chopsticks, oil-painting in the style of Van Gogh.”
- vangogh+cat: “A cat, full body, oil-painting in the style of Van Gogh.”
- sushi+cat: “A cat eating sushi with chopsticks.”
- unconditional: “”,

We used the `attention_map_diffusers` library [wooyeolbaek \(2025\)](#) to hook into SDXL’s cross-attention layers within the Down, Mid, and Up blocks. We ran with 15 inference steps total with the standard `EulerDiscreteScheduler` but extracted attention maps at intermediate times (step 1, 7, and 15 for low, mid, and high noise). To approximate the mean difference vectors for heuristic 3 we generated 10 samples per prompt and averaged the cross-attention maps, subtracting the unconditional average from each prompt average. Importantly, for each prompt, we actually selected and averaged only the specific cross-attention map corresponding to the *single token* most

---

relevant to the concept (namely: dog, horse, cat, gogh, monet, sai, sushi, croissant), and for the unconditional prompt we selected the end-of-sequence token (which we found received most of the attention). We then computed cosine similarities between the mean difference vectors for each pair of prompts. Figure 13 shows a larger version of the cosine similarity heuristic for all cross-attention layers shown in Figure 7, as well as the mid block activations at low and mid noise levels. We identify a possible structured feature-space within the first 5 cross-attention layers of the Mid block; note that this an empirical and subjective identification, but may help explain the model’s observed compositional success (see discussion in Section E.4).

For the Compositional attention analysis, we use the composite prompts listed above and compute the cosine similarity between the mean difference vector for the compositional prompt (e.g. van-gogh+cat+sushi) evaluated at a specific token (e.g. cat) and the mean difference vector for the single “cat” prompt, evaluated at the cat token.